HHS Public Access

Author manuscript

Cell Stem Cell. Author manuscript; available in PMC 2025 August 01.

Published in final edited form as:

Cell Stem Cell. 2024 August 01; 31(8): 1222–1238.e10. doi:10.1016/j.stem.2024.05.011.

Primitive macrophages enable long-term vascularization of human heart-onchip platforms

Shira Landau[1,2,*], **Yimu Zhao**[1,2,*], **Homaira Hamidzada**[2,6,7], **Gregory Kent**[3,4], **Sargol Okhovatian**[1,2], **Rick Xing Ze Lu**[1,2], **Chuan Liu**[1,2], **Karl T Wagner**[1,2,5], **Krisco Cheung**[5], **Sarah A. Shawky**[8], **Daniel Vosoughi**[2,9], **Erika Leigh Beroncal**[10], **Ian Fernandes**[3,4], **Carolyn L. Cummins**[8,11,12], **Ana C Andreazza**[10,13,14], **Gordon M Keller**[3,4], **Slava Epelman**[2,6,7,15,16,#], **Milica Radisic**[1,2,5,$,#]

[1.]Institute of Biomedical Engineering, University of Toronto, Toronto, ON, Canada

[2.]Toronto General Hospital Research Institute, University Health Network, Toronto, ON, Canada

[3.]McEwen Stem Cell Institute, University Health Network, Toronto, ON, Canada

[4.]Department of Medical Biophysics, University of Toronto, Toronto, ON, Canada

[5.]Department of Chemical Engineering and Applied Chemistry, University of Toronto, Toronto, ON, Canada

[6.]Ted Rogers Centre for Heart Research, Translational Biology and Engineering Program, Toronto, ON, Canada

[7.]Department of Immunology, University of Toronto, Toronto, ON, Canada

[8.]Department of Pharmaceutical Sciences, Leslie Dan Faculty of Pharmacy, University of Toronto, Toronto, ON, Canada

[9.]Institute of Medical Science, University of Toronto, ON, Canada

[10.]Department of Pharmacology and Toxicology, University of Toronto, Toronto, ON, Canada

[11.]Banting and Best Diabetes Centre, Toronto, ON, Canada

[12.]The Heart and Stroke Richard Lewar Centre of Excellence in Cardiovascular Research, Toronto, ON, Canada

[13.]Department of Psychiatry, University of Toronto, Toronto, ON, Canada

[#]**Corresponding Authors:** Milica Radisic, m.radisic@utoronto.ca (Lead contact), Slava Epelman, slava.epelman@uhn.ca.
[*]Co-first authors
[$]Lead contact

Author contributions

S.L., Y.Z., K.T.W., S.E., R.L., S.A.S, C.L.C and M.R. designed research; S.L., Y.Z., S.O., C.L., H.H., E.B., A.C.A R.L., and S.A.S performed research; S.L., Y.Z., K.C., D.V., H.H., E.B., S.A.S and A.C.A. analyzed data; H.H analyzed snRNA sequencing; G.M.K, I.F. and G.K. provided hESCs-derived macrophages and hESCs-derived CMs; S.L., Y.Z., and M.R. wrote the paper.

Declaration of interest:

MR and YZ are inventors on an issued patent that describes Biowire technology. This patent is licensed to Valo Health. MR and YZ receive licensing revenue.

[14]Centre for Addiction and Mental Health, Toronto, ON, Canada

[15]Peter Munk Cardiac Centre, University Health Network, Toronto, ON, Canada

[16]Department of Laboratory Medicine and Pathobiology, University of Toronto, Toronto, ON, Canada

Abstract

The intricate anatomical structure and high cellular density of the myocardium complicate the bioengineering of perfusable vascular networks within cardiac tissues. In vivo, neonatal studies highlight the key role of resident cardiac macrophages in post-injury regeneration and angiogenesis. Here, we integrate human pluripotent stem cell-derived primitive yolk-sac-like macrophages within vascularized heart-on-chip platforms. Macrophage incorporation profoundly impacted the functionality and perfusability of microvascularized cardiac tissues up to two weeks of culture. Macrophages mitigated tissue cytotoxicity and the release of cell-free mitochondrial DNA and upregulated the secretion of pro-angiogenic, matrix-remodeling, and cardioprotective cytokines. Bulk RNA sequencing revealed an upregulation of cardiac maturation and angiogenesis genes. Further, single nuclei-RNA sequencing and secretome data suggest that macrophages may prime stromal cells for vascular development by inducing IGFBP7 and HGF expression. Our results underscore the vital role of primitive macrophages in the long-term vascularization of cardiac tissues, offering insights for therapy and advancing heart-on-a-chip technologies.

Summary

Creating stable and functional vascularized cardiac tissue remains a significant ongoing challenge. Our study explored the integration of four human cell types, endothelial, stromal cells, pluripotent stem cell (PSC)-derived cardiomyocytes, and PSC-derived yolk sac-like primitive macrophages (MΦs), to form vessel networks. We generated fibrin-based tissues and employed two types of organ-on-a-chip devices, Biowire and iFlow plates, to evaluate both cardiac and vessel functionality within the generated microtissues. The vasculature persisted and functioned over a minimum of two weeks in the cardiac tissue in each embodiment: fibrin plug, Biowire and perfusable iFlow plate. Our findings indicate that primitive MΦs were critically important for the enhancement of functionality of vascularized cardiac tissues via direct cellular interactions and the secretion of matrix metalloproteinases, pro-angiogenic and cardiac-supportive factors. This method results in tissues that exhibit increased cellular viability, enhanced contractility, and perfusable, patent microvasculature within cardiac tissue.

Graphical Abstract

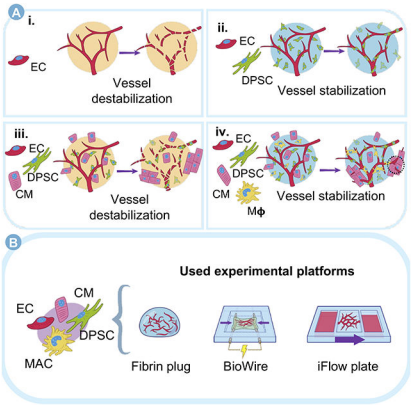

eTOC Blurb:

This study demonstrates an approach to develop vascularized cardiac tissue using a combination of human cell types and organ-on-a-chip technology. The integration of primitive macrophages significantly enhances tissue function and enables creation of stable, patent and perfusable microvasculature within cardiac tissue.

Keywords

myocardium; vascularization; resident macrophage; pluripotent stem cell; cardiomyocyte

Introduction

To satisfy its significant energy requirements, the heart tissue is highly vascularized *in vivo*[1]. In the myocardium, stromal cells, endothelial cells (ECs), and resident macrophages (MΦs) play an essential role in matrix deposition, vascularization, and paracrine signaling[2,3]. Cardiac resident MΦs seed the developing heart during embryonic development and in rodent models facilitate angiogenesis, cardiac repair post-myocardial infarction (MI), electrical conduction, and cardiomyocyte (CM) proliferation[4–7]. Yet, little is known about their role in promoting stable vascularization in the human myocardium, a question that could be addressed using human pluripotent stem cell-derived cardiac tissues.

Challenges such as poor grafting efficiency of transplanted cells and/or implanted cardiac bioengineered tissues into the myocardium are potentially attributed to the absence of sufficient vasculature. Moreover, the development of vascularized cardiac tissue could enhance disease modeling and drug testing applications. Notable advances have been made toward human cardiac tissue vascularization[8], employing organoid systems[9], synthetic scaffolds[10], cell sheet methods[11], 3D printing[12] and bioreactor cultivation to apply mechanical strain and perfusion[13]. Yet, current cardiac tissues generally lack high-density and perfusable microvasculature that is stable over weeks.

In addressing this challenge, we present a unique approach, hypothesizing that achieving cell circuit homeostasis among key myocardial cell constituents is necessary for maintaining stable perfusion within the human cardiac tissue. The establishment of cell circuits, defined

by growth factors exchange between multiple cell types, offers several advantages within bioengineered tissues, such as controlling cell population sizes, spatial organization, and regulating responses to stimuli[14]. In recent findings, fibroblasts and MΦs were shown to form a stable two-cell circuit *in vitro*, controlling cell ratios through reciprocal exchange of growth factors. This circuit's key features are likely applicable to other cell-type interactions *in vivo* and could be employed for stable vascularization of cardiac tissues *in vitro*[15].

Recent advances in human pluripotent stem cell differentiation protocols enable the derivation of human primitive MΦs from cells representing a yolk sac mesoderm[16]. We posit that primitive MΦs represent the correct source of cells for integration into human cardiac tissue, due to their potential resemblance to the earliest MΦs that seed the heart during development[17,18]. Thus, we hypothesize that incorporation of primitive MΦs along with stromal cells, CMs and ECs is critical to achieving a functional, engineered vascularized human cardiac tissue that will be stable for prolonged time periods and allow functional maturation of vascularized cardiac tissues.

Our results demonstrate that primitive MΦs enhance vascularized cardiac tissue performance via two primary mechanisms: direct cellular interaction and the release of matrix metalloproteinases (MMPs) alongside other pro-angiogenic and cardiac-related cytokines, resulting in long-term perfusable tissues with increased cellular viability and improved tissue function.

Design

Our objective is to construct a vascularized cardiac tissue that is stable over a period of weeks and where both cardiac and vasculature functions are maintained. The key design criterion is enhancing the fidelity of cellular composition. Thus, the challenge includes selecting the cell types and ratios that enable recreation of a vascularized cardiac niche. Whereas the combination of endothelial cells (EC), a stromal cell type (dental pulp stem cells DPSC) and iPSC-derived cardiomyocytes (CMs) enables a short-term vascularized tissue formation, the vessels regress in days. Consequently, we chose to integrate primitive macrophages (MΦs), which are akin to cardiac resident macrophages that are known to support both vascular and cardiac functions *in vivo*. This cell combination can be easily assessed within a simple 3D environment *in vitro* via cultivation in a fibrin hydrogel. Given that cardiac function cannot be fully and accurately assessed within the fibrin hydrogel, a cardiac platform that allows precise functional measurements is needed. For this purpose, we utilized the Biowire platform, comprising two elastomeric wires set within a polystyrene well. This setup enabled non-invasive assessment of cardiac function.. However, the Biowire platform does not support the assessment of perfusable vasculature. Therefore, we utilized the iFlow plate, a 384-well platform consisting of three compartments connected by channels to induce and maintain perfusable vasculature, and within this platform, we assessed the cell combinations as well. This design enabled the integration of primitive MΦs into cardiac tissue to support vascularization and cardiac function *in vitro* across all three methodologies.

Results

Co-culture of endothelial and stromal cells enables microvasculature formation

The requirement for co-culturing pericyte-like supporting cells with ECs to establish a stable vasculature *in vitro* has been well documented previously[19]. Using a fibrin hydrogel, we co-cultured human umbilical vein endothelial cells (HUVECs) and human dental pulp stem cells (DPSCs). DPSCs are well-known for their effective support in vessel formation and stabilization when compared to other supporting cells, such as mesenchymal stem cells (MSCs) or fibroblasts, making them an ideal choice for this study[20,21] (Figure 1a).

As expected, when DPSC were absent only a few microvessels formed in EC monoculture, demonstrated by imaging (Figure 1b) and vessel's elements quantification (Figure S1): eccentricity (a measure of how much a conic section deviates from being circular) as an indicator for vessel elongation, number of junctions and average vessel length (Figure 1c–e). DPSCs expressed α-smooth muscle actin (αSMA) (Figure 1f), a marker of recruited pericytes[22], and secreted collagen IV (Figure 1g), a basement membrane protein, around the vessels. ECs co-cultured with DPSCs expressed CD105 (Figure 1h), a TGFβ receptor expressed in angiogenic ECs[23]. Bulk-RNA sequencing of the two groups revealed upregulated genes and enriched pathways related to collagen synthesis and extracellular matrix (ECM) organization, emphasizing the importance of the tissue environment in vessel stabilization (Figure 1i–m and Supplemental Table 1). PDGFR-β was upregulated within the co-culture group, suggesting the recruitment of DPSCs to serve as pericytes and allow for vessel stabilization[24]. TGFβ1, a pericyte phenotype regulator that also stimulates ECM production[25], was another upregulated gene (Figure 1i–m).

CMs, ECs and stromal cells in combination insufficiently support stable microvascularization of cardiac tissues

We then further included human-induced pluripotent stem cell (iPSC) derived CMs to the EC/DPSC co-culture to develop vascularized cardiac tissues. The presence of CMs interfered with cellular homeostasis and resulted in vessel regression (Figure 2a–b). Quantification of vessel elements, including average vessel length, number of junctions, and mean lacunarity (a measure of the distribution of gaps of different sizes in a fractal or multi-scale object), confirmed the findings (Figure 2d–f). To verify that this phenomenon is not cell-source dependent, we also used human embryonic stem cell (hESC)-derived venous endothelial cells (VEC) and hESC-derived CMs (both from HES2 line), observing a similar trend, although at a different rate. Vessels formed at an earlier time point (day 8) and disrupted at a later time point (day 18) (Figure S1b).

Bulk RNA sequencing revealed the upregulation of genes and enriched pathways related to cardiac and muscle function in tissues with CMs, as expected. Importantly, some of the downregulated genes were angiogenesis-related, including hepatocyte growth factor (HGF), matrix metalloproteinase (MMP)9, angiopoietin-like protein (ANGPTL)4, and transforming growth factor TGFβR-3. Thus, the inclusion of CMs in the co-culture of ECs and stromal cells leads to gene expression dysregulation that may disrupt cell circuit homeostasis (Figure 2g–j and Supplemental Table 1).

To exclude the possibility that our findings were a result of insufficient cell ratio optimization, we seeded a gradient of CM percentages, specifically, 0:50:50, 30:35:35, 50:25:25 and 70:15:15 of CM:EC:DPSC tracking vessel formation over time. The cell ratios employed in this experiment align with previous studies, wherein the CM population constituted approximately 60% of the total cell population in a vascularized cardiac organoid system[9] and approximately 50% in the adult human heart[26,27]. In both cases, the cell number of ECs and fibroblasts was approximately equivalent. Vessel regression increased with the increased percentage of CMs in the culture, as shown by imaging of vessel elements and junctions. Cardiac troponin-T (TnT) staining and beating amplitude showed a positive correlation with the concentration of CMs (Figure S1ci–iii), as expected.

To rule out the possibility that vessel disruption was due to high cell density within the tissues, we increased the number of DPSCs co-cultured with HUVECs to match the total cell density present in the tri-culture studies above, but our results showed no reduction or regression of the vessels within this group, suggesting that another mechanism is causing regression in CM co-cultures (Figure S1d). The role of DPSC as mural cells was also evident when adding CMs to the culture. ECs co-cultured with CMs without DPSC supporting cells tended to form a monolayer structure without any observable vessels (Figure S1e).

Incorporation of hESC-derived macrophages promotes microvascularization of cardiac tissues

Macrophages (MΦs) were differentiated from hESC hematopoietic progenitors (Figure 3a). These cells expressed canonical MΦ lineage markers, including CD45, CD14, CD64, and CD68, and were negative for CCR2, a marker for monocyte and monocyte-derived MΦs (Figure 3b and S2a and b). They were lymphatic vessel endothelial hyaluronan receptor 1 (LYVE1) positive, a key marker for embryonic-derived primitive MΦs (Figure 3c). From bulk RNA sequencing, we identified markers known to be associated with the resident macrophage phenotype (list adapted from[28,29]), noting a significant expression of the following genes: *MRC1, CD163, F13A1, FOLR2*, and *LYVE1* (Figure 3d) in the MΦs used for co-culture experiments. Resident MΦ gene signatures are often overlapping with “M2-like” patterns, and as expected, we observed that MΦs co-cultured with EC/DPSC/CM expressed *MRC1, CD163, F13A1, CD86*, and *CD209* (Figure 3d). Overall, these markers suggest that these cells possess a similar gene expression profile as resident TLF+ cardiac MΦs described previously[4,29,30].

In groups where primitive MΦs were added to the tri-culture of ECs/DPSCs/CMs (Figure 3e), vessel stabilization occurred, with intact vasculature for up to 2 weeks and a higher vessel density, junction number, and length, as well as a lower mean lacunarity (Figure 3f–l and S2c and d). Primitive MΦs physically interacted with the vasculature, wrapping around the vessels or bridging between them (Figure 3h and S2e). Brightfield imaging revealed more uniform tissue formation within the group containing MΦs (Figure 3f and S2d). Histological staining for H&E and CD31 demonstrated a more connected vasculature within the tissues with MΦs, in contrast to the tissues without MΦs, which displayed a more fragmented vessel network (Figure 3m and S2c).

Studies with iCell CMs (iCMs) provided similar trends as those with BJ1D induced pluripotent stem cells (iPSC) derived CMs, confirming the findings were not cell source dependent (Figure S3a and b). Transwell experiments demonstrated a decrease in the positive effect of MΦs on vessel formation compared to MΦs mixed within the culture, as indicated by a lower vessel density (Figure S3c and d), confirming the requirement for cell contact. MΦs not only enhanced vessel stabilization but also supported cardiac function (Video S1a and b) through synchronization of spontaneous beating (Figure 3q and Video S1a and b) despite only slightly denser TnT staining (Figure 3n–p).

The incorporation of primitive MΦs enhances the contractility of vascularized cardiac tissues

To further investigate the effect of primitive MΦs on cardiac tissue function, we employed the Biowire heart-on-chip platform (Figure 4a). The polymer wires within the system enable optical assessment of contractility using the calibrated wire deflection. After seeding, tissues from both groups compacted well and stabilized after 14 days in culture (Figure 4b). Biowires with MΦs had a more uniform tissue structure (Figure 4b, c and S4f). H&E staining confirmed denser and more intact ECM in tissues with MΦs Figure 4c), whereas CD31 staining and live imaging of GFP-tagged ECs showed elongated and connected vessel formation with MΦs, in contrast to the aggregated ECs and segregated vessels observed in tissues without MΦs (Figure 4d and e). CD68 staining confirmed the presence of MΦs after two weeks of culture (Figure 4f). Confocal images of tissues with MΦs demonstrated a more elongated and interconnected vasculature (GFP+) colocalized with CMs (MLC2v) (Figure 4f), which was drastically different from tissues without MΦs. Sarcomeric α-actinin staining demonstrated highly dense and striated CMs, consistent with the tension exerted by the Biowire platorm[31] (Figure 4g and j). Although the excitation threshold (ET) was not significantly different between the week 1 and week 2-time points for each group, quad-culture tissues with primitive MΦs initially presented a higher ET than an additional control, tissues consisting of only CMs and DPSC (Figure 4h and S4a). The maximum capture rate (MCR) of quad-culture was significantly higher at both time points when compared to the two control groups (Figure 4i and S4b). When normalized to input CM number, quad-culture tissues incorporating primitive MΦs demonstrated a significantly higher force of contraction than the group without MΦs (Figure 4j, S4c, Video S1c, Video S1c). There were no significant differences in the tissue diameter, indicating a similar compaction rate (Figure S4e), and supporting the conclusion that force differences are not driven by changes in the tissue diameter, rather than the changes in the cells themselves. The presence of α-actinin was only slightly increased with the inclusion of MΦs (Figure 4k), further supporting that the force differences are not the result of the profound differences in CM fraction, but the enhanced overall cell health in the tissues with MΦs.

The CM/DPSC group served as a baseline control, allowing the assessment of the ECs and MΦs addition on the functional properties (Figure S4a–e). Most notably, the CM/DPSC control demonstrated that the inclusion of ECs to the mixture of CM/DPSC resulted in a profound decline of active force (Figure S4c and d) and the impediment in tissue compaction (Figure S5e) at week 2. These effects were fully rescued by the inclusion of primitive MΦs, resulting in further functional improvements (Figure S4c, d and e). As expected at earlier

time points (week 1), the addition of more non-myocytes in the groups with MΦs hampered electrical excitability parameters such as excitation threshold (Figure S4a); by week 2, tissues with MΦs improved measures of electrical excitability (e.g. maximum capture rate) over all other control groups (Figure S4b).

We further demonstrated the feasibility of a sequential seeding technique, where EC/DPSC core is generated first, followed by the seeding of CMs with and without MΦs two days later to create Biowires with two layers, inner vascular layer, and outer cardiac layer, which eventually integrate over time in culture (Figure S4f and g). We postulated that seeding CM on top of already pre-formed vascular layer could exert additional benefits. In sequential seeding, the tissues containing MΦs exhibited a trend similar to simultaneous seeding, with a lower excitation threshold by day 14 (Figure S4h), an increased maximum capture rate on day 14 (Figure S4i), a trend of higher active force (Figures S4j and k), and a marginally reduced tissue width (Figure S4l). The ratio of active/passive force was higher with MΦs in sequentially seeded tissues (Figure S4k).

The incorporation of primitive macrophages enables perfusion of microvascularized cardiac tissues

To assess vascular function, specifically perfusability, we used the iFlow plate (Figure 5a and b). To further characterize our vascular model before adding CMs, we also conducted an iFlow plate experiment using only EC/DPSC (Figure S5a). Cardiac tissues with MΦs exhibited intact, perfusable vasculature, with Rhodamine-Dextran (Figure 5c) and 405-polystyrene (PS) beads (Figure 5d and Video S2a) flowing through the vessels. No leakage of dextran or PS beads was observed in this group, remaining stably within the vessels (Figure 5c and d, Video S2a) and with 100% of perfusable tissues (Figure 5e). The permeability of the cardiac tissue vessels with MΦs was similar to a range of physiological values (Figure 5f).

Tissues without MΦs showed impaired perfusability, with only 25% of tissues achieving a perfusable vasculature (Figure 5c–e), the great majority remaining as a slab of non-perfusable hydrogel demonstrated by the inability of Rhodamine-Dextran and PS beads to flow into the structure (inset images in Figure 5c and d, EC/DPSC/CM group) and lower functional vessel density (Figure f). TnT staining demonstrated a clear abundance of CMs in the tissues with close apposition to the endothelial cells lining the vessels (Figure 5h and i).

The vessels in EC/DPSC/CM group were more patent (i.e. less permeable) than those in the vasculature only (EC/DPSC) benchmark (Figure S5a). This is expected since cardiomyocytes contribute an additional layer, thus increasing the vessel's barrier. Yet, both values (Figure S5a) fall within the physiological range and align with previously reported permeability for in vitro perfusable vasculature[32]. Moreover, they are lower than the previously reported permeability values for tumor vasculature with 70 kDa dextran, which is estimated to be around 1×10^−6[33].

We then aimed to examine whether MΦs exert distinct effects when cultured with cardiac organoids compared to single-cell CMs (Figure S5b–d, Video S2b and c). A higher density of perfusable vessels and a lower permeability were observed in hESC-organoid tissues

co-seeded with primitive MΦs (Figure S5d, Video S2c). Perfusable vasculature was limited when cardiac organoids were grown with EC/DPSC in the absence of primitive MΦs (Figure S5b–d, and Video S2b). Instead, superfusion and interstitial flow were observed (Video S2b). Consequently, the tissues without MΦs exhibited impaired barrier function, which is evident by a higher permeability (Figure S5d). TnT density did not show a statistical difference (Figure 5g). This is consistent with the staining quantification from both the fibrin tissue and the Biowire.

The incorporation of primitive macrophages decreases the release of cell-free mitochondrial DNA and lactate dehydrogenase injury markers

Given the considerable mechanical stress and metabolic requirements imposed on CMs by the constant rhythm of the heart, the capacity of these enduring cells, which rarely regenerate, to independently maintain homeostasis of their environment remains elusive. To address this, we analyzed the secretion of cytotoxicity markers. The release of cell-free mitochondrial DNA (mtDNA) within the culture supernatant was reduced as detected by ND1 and ND4 from tissues containing primitive MΦs (Figure 6a). The secretion of lactate dehydrogenase (LDH), a general marker of cell damage and one of the clinical markers of cardiac injury[34], into the culture media was significantly lower from the quad-culture tissues with primitive MΦs (Figure 6b). Collectively, these data indicate that cell damage and death in vascularized cardiac tissues are decreased in the presence of primitive MΦs.

Secretion of angiogenic, matrix remodeling and cardioprotective cytokines is enhanced in tissues with primitive macrophages

Upon analyzing 504 cytokines using an antibody array on media collected on day 10 of culture, an asymmetrical volcano plot emerged, a result anticipated due to the inclusion of primitive MΦs in one of the groups, known for their abundant cytokine production (Figure 6c). Among the most significantly released cytokines, we detected pro-angiogenic cytokines: MMP-12, a potent mediator in vascular homeostasis[35]; MMP-2, which allows matrix degradation and was previously shown to form a stable complex with integrin αvβ3, which allows ECs motility, crucial for vessel development[25], and angiopoietin-like 1, that interacts with ANGPTL2 to facilitate angiogenesis[24]. Moreover, angiopoietin-2, released by perivascular MΦs, enhances vessel destabilization to facilitate stimulation of sprouting[24]. Among the cardio-protective up-regulated cytokines was NRG-3, known for its crucial role in the regulation of cardiac homeostasis[36], and SIGIRR, a suppressor of interleukin-1 (IL-1) receptor/Toll-like receptor signaling. Previous studies have shown that inflammation was increased in SIGIRR-deficient mice[37]. Another upregulated cytokine was adiponectin, which facilitates cardiovascular homeostasis by enhancing vasodilatory, anti-apoptotic, anti-inflammatory, and anti-oxidative effects on both CMs and ECs[38]. (Figure 6d)

A proteomic analysis of the conditioned media collected on day 10 of culture and protein interaction network analysis revealed that the upregulated secreted proteins were primarily associated with hemostasis and ECM formation, specifically basement membrane components, and cell adhesion molecule binding. These findings demonstrate the contribution of MΦ to conditioning the cell microenvironment to support the establishment of homeostasis among the four cell types (Video S3)

Bulk RNA sequencing demonstrates enhanced gene expression of pro-angiogenic and cardiac markers in vascularized tissues with primitive macrophages

The volcano plot of differentially expressed genes between EC/DPSC/CM/MΦ and EC/DPSC/CM groups showed mostly upregulated genes, which was expected due to the additional cell population in quad-culture (Figure 6e and f and Supplemental Table 1). Gene expression data demonstrated that the addition of primitive MΦs had a positive effect on both cardiac tissue and vessel function genes (Figure 6g and Video S4). Gap junction genes were also elevated when MΦs were present in the culture, with an increase in the expression of *GJA3* and *GJA4* (Figure 6h).

To select cardiac-related genes, an unsupervised hierarchical clustering of the three groups (EC/DPSC/CM/MΦ, EC/DPSC/CM, and EC/DPSC) was performed according to the genes that were upregulated in the EC/DPSC/CM versus EC/DPSC group (Figure 6i and S6a). Pathway enrichment analysis of the selected genes revealed that only the upregulated genes were related to cardiac function (Figure 6j and S6b).

Notable upregulation of several critical cardiac genes, including *SCN5A, MYH6, ACTC1, TNNI1, NPPA, MYOCD, MYLK3, MYOZ2, MYL4, MYZAP, MYOM1* were driven by the presence of primitive MΦs. This also includes *TNNI1*, which plays a fundamental role in the contraction of cardiac muscle, and *SCN5A*, a gene associated with upstroke velocity. Finally, *ACTC1* encodes the cardiac muscle-specific isoform of actin, an essential component of the cardiac contractile apparatus (Figure 6k).

Collagen expression showed a completely different pattern between the two groups, where tissues without primitive MΦ expressed various types of collagens such as *COL1A1* and 2, which in some instances could be related to fibrosis. In contrast, the tissues with primitive MΦ had a significantly higher expression of *COL4A5* and 6, basement membrane components (Figure S6c and d), another indicator of enhanced stabilization of the forming vasculature.

Other components that were significantly increased within the MΦ-containing vascularized tissues were MMPs, specifically, MMP-9,−10 and −12. MMPs have an important role as matrix degradation enzymes that allow EC growth and new sprouting within an existing vasculature. Tissues without primitive MΦs on the other hand, had higher expression of TIMPs, MMPs inhibitors (Figure S6e). Both TIMP-1 and −2 have been reported to have a negative effect on angiogenesis[39]. Overall, these results highly correlate with the observational results showing intact and stable vessels in the presence of MΦs.

snRNA-seq profiling reveals macrophages promote pro-angiogenic pathways in stromal cells

Since bulk RNA sequencing does not allow us to determine cell-type specific gene expression and to eliminate the issues of dilution of the RNA pool upon MΦ incorporation, we conducted single nucleus RNA sequencing (snRNA-seq) on two groups, EC/DPSC/CM, and EC/DPSC/CM/MΦ, as well as the initial MΦs population to dissect intercellular communication and downstream pathways induced in ECs, CMs and stromal cells driven by the presence of MΦ.

The combined analysis of 33,514 cells in EC/DPSC/CM and EC/DPC/CM/MΦ groups revealed 8 populations, including EC, DPSC, MΦ, and CM (Figures 7a–c). We identified two subpopulations of CMs, a less mature CM1 and a more mature CM2. CM2 expressed higher levels of mature sarcomeric genes, including *MYH7, TNNI3, MYL2* and *RYR2* (Supplemental Table 2). The identified population of cardiac fibroblasts-FB, likely arose from the cardiac differentiation protocol, known to yield some FB contamination.[40] Two additional clusters that appeared to be transcriptionally similar to CM1 or CM2, also expressed overlapping signatures with EC, DPSC and fibroblasts, therefore we termed them unclassified 1 and 2 (Figure 7b).

We identified 1925 upregulated and downregulated DEGs in DPSCs and 1007 upregulated and downregulated DEGs in FBs, as a result of MΦs presence (Supplemental Table 3). Angiogenesis pathways, crucial for the formation and functionality of vasculature, were significantly activated in DPSCs and FBs in tissues with MΦs despite being downregulated in CMs (Figures 7d and e). The macrophage orchestration of pro-angiogenic phenotype in the stroma may further be suggested by the upregulation of *HGF* in DPSC and *IGFBP7* in DPSC and FBs (Supplemental Table 3), markers consistent with a proangiogenic phenotype in mural cells[41].

Next, we performed receptor-ligand interaction analysis to assess intercellular communication between the engineered tissues' cellular components driving transcriptional differences. We used NicheNet[42] in order to prioritize receptor-ligand interactions based on the expression of target genes in recipient cells. This analysis revealed a complex network of interactions between ECM components secreted by MΦs and various integrins on the surface of recipient cells, hinting at a MΦ-mediated enhancement in cell adhesion to the ECM and subsequent cell migration, which are fundamental to angiogenesis. Specifically for EC receptors and MΦ ligands, focal adhesion components *ITGA5, ITGA2, ITGAV, ITGB1*, and *CD44* on ECs were inferred to interact with fibronectin (*FN1*) expressed by MΦs. This implies the interaction of α5β1, α2β1 and αvβ1 integrins with fibronectin. (Figure 7f–i).

In addition to the expected interaction between integrin receptors and ECM proteins, which is broadly required for cell adhesion and migration required for angiogenesis, our analysis suggests a role for semaphorin 3A (*SEMA3A*), which has been shown to bind to Neuropilin 1 (NRP1) (Figure 7f and g). We observed an interaction involving *NRP1* expressed on CMs and *SEMA3A* expressed by MΦs (Figure 7i).

Secretome analysis enabled us to further focus on signaling via ligands confirmed to be secreted into the culture media, identifying 39 upregulated in both snRNA and proteomics (Figure 7j). Upon analyzing the enriched pathways related to these genes in DPSCs, FBs, and ECs (Figure 7k–m), they were associated with cell adhesion, migration, focal adhesion, VEGFA signaling, ECM organization, and actin-binding, underscoring the influence of MΦs on vascular stabilization (Figure 7n–p).

Mapping their p-values and fold changes from both snRNA sequencing (Figure 7q) and proteomics data (Figure 7r), we found that HGF, predominantly secreted by DPSCs, and IGFBP7, primarily secreted by both FBs and DPSCs, with a minor contribution from ECs,

were upregulated. These factors are essential for the formation of luminalized vasculature. Laminin Subunit α2 (LAMA2), mainly produced by FBs with a minor release from ECs, and Collagen Type IV α2 Chain (COL4A2), also secreted predominantly by FBs and to a lesser extent by ECs, constitute significant components of the basement membrane. Additionally, Filamin B (FLNB), mainly secreted by FBs and to a lesser degree by ECs, Clathrin Heavy Chain (CLTC), and Annexin A1 (ANXA1), both secreted by DPSCs and FBs, along with A Disintegrin and Metalloproteinase Domain 10 (ADAM10) from FBs, Syndecan (SND) from DPSCs and ECs, EWS RNA Binding Protein 1 (EWSR1) from DPSCs, and IGFBP play a vital role in VEGFA signaling (Figure 7q).

Additionally, we assessed whether phenotypic changes occur in MΦs seeded in tissues relative to those cultured alone in suspension, by snRNA-seq analysis of the initial MΦ population relative to EC/DPSC/CM/MΦs. The tissue resident MΦs gene signature is known to track with “M2-like” transcriptional programs. In both conditions, the expression of genes associated with tissue resident MΦs were identified, and a lack of inflammatory genes often seen in “M1-like” transcriptional programs (Figure S7b and c).

We generated MΦs-specific signature using the set of upregulated differentially expressed genes in MΦs relative to all other cell types present in quad-cultured tissues, i.e. EC/DPSC/CM/MΦs. We then scored macrophages from suspension (MΦs) or quad tissues (EC/DPSC/CM/MΦs) using this gene set and found that macrophages residing in the tissues were transcriptionally distinct from those in suspension and significantly upregulated this tissue-specific signature (Figure S7d and Supplemental Table 4). Collectively, these results underscore the potential for MΦs to influence the formation and stabilization of vascular networks within engineered tissues via enhancement of the pro-angiogenic capacity of stromal cells while concurrently enhancing their own tissue-resident signature.

Discussion

Our findings provide insights into the role of primitive MΦs on the establishment of human vascularized cardiac tissues and underscore the importance of considering the complex interplay between different cell types in culture. The use of human cells *in vitro* necessitates employment of multiple culture configurations to prove that our findings are not an artifact of the cultivation system. Here, primitive MΦs robustly enhanced vascularization in 3D fibrin hydrogel-based tissues, and two established organ-on-a-chip systems, Biowire and iFlow plate.

One strategy to achieve active perfusion within cardiac tissues is by creating lumenized structures from synthetic materials and seeding CMs around them[43 44]. Yet, establishing spontaneously forming, perfusable, microvasculature within these models remains a significant obstacle. To date, only limited long-term stability has been achieved in microvascularization of cardiac tissue-on-a-chip platforms, with perfusion possible for only one week on average[45]. Here, we addressed this challenge by incorporating primitive MΦs to achieve functional vascularized cardiac tissue that remains stable and perfusable for extended periods.

Cardiac resident MΦs were recently shown to possess robust phagocytic activity by internalizing materials secreted primarily by CMs, including expelled mitochondria[46]. In vasculature-free cardiac tissues, the incorporation of primitive MΦs led to improved cardiac tissue development, maturation, and function, attributed to the early remodeling efforts and the reduction of cardiomyocyte death, facilitated by the macrophages' ingestion of apoptotic CM debris through a phosphatidylserine-dependent mechanism[47]. MΦs were differentially educated within cardiac microtissues by both CMs and fibroblasts, suggesting cell-type specific imprinting. Our results in vascularized tissues concur with these findings, highlighting the crucial role of MΦs in regulating vessel formation and stability, attenuating cytotoxicity as measured by mtDNA and LDH levels and the requirement for direct incorporation of the MΦs with the forming vasculature to exert this effect.

Angiogenic sprouting is tightly regulated by a balance between activators and inhibitors. A well-known inhibitor, angiostatin, suppresses the proliferation and migration of ECs[25]. Interestingly, our findings revealed that MMP-12 and angiostatin were significantly upregulated cytokines within MΦs-containing tissues. Previous research has shown that MMP-12 also converts plasminogen to angiostatin, impeding angiogenesis[25]. This highlights a complex picture, with the upregulation of anti-angiogenic genes and secreted cytokines that are necessary for vessel stabilization. Also, there was an upregulation of pro-angiogenic factors, including MMP-2, crucial for sprout formation[24].

COL1A1 and 2 were downregulated in tissues with MΦs, correlating with a recent study demonstrating that upon MΦ depletion and following cardiac pressure overload induced by transverse aortic constriction, enhanced fibrosis occurred through myofibroblast differentiation and collagen production[48]. The same study demonstrated the contribution of cardiac resident MΦs to angiogenesis[48].

The snRNA sequencing data suggest that macrophages may precondition DPSCs and FBs towards a proangiogenic state, as evidenced by the upregulation of HGF in DPSCs and IGFBP7 in both DPSCs and FBs. These results align with the characteristics of mural cells in promoting angiogenesis in vitro[41]

We also noted a crucial interplay between integrins and fibronectin, pivotal for EC migration[49] and proliferation[50]. These interactions are essential for angiogenesis, and their disruption has been shown to cause vascular and cardiac abnormalities in murine models[51]. Our investigation into SEMA3A's involvement, particularly its interaction with NRP1, adds to its previously reported role in angiogenesis, cell survival, and invasion[52,53]. SEMA3A's facilitation of blood vessel remodeling has been implicated in the formation of a mature vascular network, a process vital beyond the early developmental stages of angiogenesis[54].

Limitations of the Study

A limitation of the work presented here includes the absence of a direct assessment of the effects of primitive MΦs on the electrophysiological properties and metabolism that may underpin the improvements of some of the functional properties observed here. Due to the complexity of the culture involving four cell types, we aimed to use cells that are well-

validated and have stable phenotypes. This approach helps eliminate the potential impact of cell immaturity or variable differentiation efficacy on the vascularization study outcomes. Consequently, we employed well-established stromal cells (DPSCs) and endothelial cells (HUVECs), which have been confirmed to support stable vascularization of other tissues in numerous studies[55–57]. Future studies with isogenic cells are required.

To demonstrate the beneficial effects of the co-culture system on cardiac function, cell transplantation following myocardial infarction or ischemia-reperfusion injury is necessary. Previous research focusing on resident native MΦs shows that following cardiomyocyte ablation or myocardial infarction in neonatal mice[58,59], resident MΦs proliferate and are essential for scarless repair, angiogenesis, and cardiomyocyte proliferation[60,59,61]. Future studies will determine whether the primitive MΦs used here will adopt angiogenic or pro-fibrotic roles after injury in vivo. Further investigation may also be needed to fully understand the effects of physical stimuli (e.g., electrical or mechanical) on the tissues containing resident MΦs.

In conclusion, this study provides evidence that the addition of MΦs to a co-culture of ECs, DPSCs, and CMs promotes vessel stabilization and improves both vascular and cardiac tissue functions.

STAR METHODS

Lead contact

Further information and requests for resources and reagents should be directed to and will be fulfilled by the lead contact, Milica Radisic (m.radisic@utoronto.ca).

Materials availability

This study did not generate new unique reagents.

Data and code availability

Data

- Single-cell and bulk RNA-seq data have been deposited at GEO and are publicly available as of the date of publication. Accession numbers are listed in the key resources table. The mass spectrometry proteomics data have been deposited to the ProteomeXchange Consortium (http://proteomecentral.proteomexchange.org) via the PRIDE partner repository[62] with the dataset identifier PXD044560 and are publicly available as of the date of publication, Accession numbers are listed in the key resources table.
- All other reported in this paper will be shared by the lead contact upon request.

Code—All original codes are published. References are listed in the key resources table.

Experimental Model and Participant Details

Cell Lines

iCell: iCell cardiomyocytes (Female) were purchased from FUJIFILM and used according to the manufacturer's instructions.

hPSC venous endothelial cell: hPSC populations (HES2, female) were dissociated into single cells (TrypLE, ThermoFisher) and re-aggregated to form EBs in StemPro-34 media (ThermoFisher) containing penicillin/streptomycin (1%, ThermoFisher), L-glutamine (2 mM, ThermoFisher), transferrin (150 mg/ml, ROCHE), ascorbic acid (50 mg/ml, Sigma), and monothioglycerol (50 mg/ml, Sigma), ROCK inhibitor Y-27632 (10 uM, TOCRIS) and rhBMP4 (1 ng/ml, R&D) for 18h on an orbital shaker (70 rpm). On day 1, the EBs were transferred to mesoderm induction media consisting of StemPro-34 with the above supplements, excluding ROCK inhibitor Y-27632 and rhBMP4 (3 ng/ml), rhActivinA (1 ng/ml, R&D) and rhbFGF (5 ng/ml, R&D). On day 4, the EBs were harvested, dissociated into single cells (TrypLE), and replated as a monolayer with a density of 3 ×106 cells/10 cm plate in venous endothelial specification medium containing media consisting of StemPro-34, rhbFGF (30 ng/ml, R&D), rhVEGF (30 ng/mL, R&D) and GSI (10uM, TOCRIS). On day 8, the monolayers were dissociated (TrypLE, 6 mins, RT), and then stained for CD34 MACS (Miltenyi, 130-146-702) using 10 uL antibody/5 × 106 cells/100 uL in base media supplemented with DNAse (1 KU/mL, Millipore) for 30 min at 4 degrees C. The cells were purified over two columns in series (either MS or LS depending on cell number) to isolate populations consisting of 95% CD34+ cells or greater. The CD34+ cells were cryopreserved (Cryostore CS10, STEMCELL Technologies) at this stage for future studies. Cultures were incubated in a low oxygen environment (5% CO2, 5% O2, 90% N2) for the entire culture period.

MΦs differentiation: For MΦs differentiation, tdRFP variant of the HES2 human embryonic stem cell (hESC) line was differentiated into CD43+ primitive hematopoietic progenitors as previously described[63]. CD43+ primitive progenitors were isolated using magnetic-activated cell sorting (MACS) and cultured in suspension with media containing MCSF (30ng/mL), IL3 (50ng/mL) and SCF (100ng/mL) for 3 days followed by MCSF (30ng/mL) alone for 18+ days. *Macrophages were provided by the Keller lab (soon to be published).*

BJ1D CMs: For cardiac differentiation BJ1D iPSC (Male) were routinely maintained in matrigel coated 6-well plate in mTesr plus media and were differentiated into CMs based on previously reported protocol. Briefly, BJ1D iPSCs were preplated in 12-well plate at 0.75million cells per well and maintained in mTesr plus media for 24–48 hrs until 100% confluence. RPMI supplemented with B27 (no insulin), pen-strep and CHIR (8uM) were added on day 0 and CHIR was removed after 24 hrs incubation. IWP4 were added on day 3 and removed after 48 hrs incubation. The culture were maintained in RPMI with B27 (no insulin) until day 7 and switched to the RPMI with B27 for the rest of the culture time. CMs were harvested by incubating cells with 10X tryplE for 15–30 mins at 37C.

Primary Cultures—HUVEC (Angioprotemie), were cultured in EGM2 media (ScienceCell). DPSCs (Lonza) were cultured in low-glucose DMEM, 10% FBS, 1% NEAA, 1% GlutaMAX, and 1% Pen strep, with a media change every two days.

Method Details

Flow cytometry—MΦs were stained with the following antibodies for 30 minutes at 4 degrees C: mouse anti-human CD45 (1:100, BioLegend Cat#304042 RRID: AB_2562106), mouse anti-human CD14 (1:100, BioLegend Cat# 301814 (also 301813), RRID:AB_389353), mouse anti-human CD64 (BioLegend Cat#305026, RRID: AB_2561588), mouse anti-human CD68 (BioLegend Cat#333816, RRID: AB_2562936), and mouse anti-human CCR2 (1:100, BioLegend Cat# 357207 (also 357208), RRID:AB_2562238). Cells were washed in PBS with 2% bovine serum (1mM EDTA) and centrifuged for 5 minutes at 400g (4 degrees C). Cells were resuspended in PBS with 2% bovine serume (1mM EDTA) and acquired on the BD LSRFortessa.

3D tissue formation based on 3D fibrin hydrogel (Method S1)—Three-dimensional vascularized cardiac tissues based on fibrin hydrogel were obtained by seeding of four cell type with different combinations as follows:

1. GFP-tagged HUVEC (100%) monoculture, with 1.6M HUVEC/ml
2. GFP-tagged HUVEC/DPSC in the ratio of 50:50, with 1.6M HUVEC/ml and total concentration of 3.3M cells/ml
3. GFP-tagged HUVEC/DPSC/CMs tri-culture in the ratio of 25:25:50, with 1.6M HUVEC/ml and total concentration of 6.6M cells/ml
4. GFP-tagged HUVEC/DPSC/CMs/RFP-tagged MΦs quad-culture in the ratio of 20:20:40:20 with 1.6M HUVEC/ml and total concentration of 8.3M cells/ml.

For the gradient increase of CM number experiment, the following cell combinations were used with total cell concentration of 11.6M cells/ml for all groups:

1. GFP-tagged HUVEC/DPSC in the ratio of 50:50
2. GFP-tagged HUVEC/DPSC/CMs tri-culture in the ratio of 35:35:30
3. GFP-tagged HUVEC/DPSC/CMs tri-culture in the ratio of 25:25:50
4. GFP-tagged HUVEC/DPSC/CMs tri-culture in the ratio of 15:15:70

For increased concentration of DPSC two cell combinations were used:

1. GFP-tagged HUVEC/DPSC/CM tri-culture in the ratio of 17:50:33 with total cell concentration of 10M cells/ml and with 1.6M HUVEC/ml
2. GFP-tagged HUVEC/DPSC/CM tri-culture in the ratio of 25:25:50 with total cell concentration of 6.6M cells/ml and with 1.6M HUVEC/ml

The indicated cell combinations were suspended in 9µl human fibrinogen (30mg/ml, Sigma-Aldrich) within a 350µl tube, and mixed with 3µl of human thrombin (33U/ml, Sigma-Aldrich) to achieve a 12µl fibrin tissue, the tissue was placed in a middle of a 12 well plate,

followed by a 30-min incubation before the addition of culture medium. 50% EGM2 mixed with 50% I3M media (StemPro-34 complete media supplemented with 20mM HEPES, 1% GlutaMAX, and 213ug/mL 2-phosphate ascorbic acid) then 500ul media was added slowly to prevent tissue rupture. Fibrin based tissues were cultured for up to 14 days and media was changed every two days.

Biowire II tissue preparation and culture (Method S2)—Biowire II chips were fabricated with patterned polystyrene sheets and poly octamethylene maleate (anhydride) citrate) (POMaC)-based wires according to the previously reported method[31]. The following cell combination were used:

Simultaneous seeding

1. DPSC/CMs co-culture in the ratio of 1:5 ratio with total cell concentration of 50M cells/ml.
2. GFP-tagged HUVECs/DPSCs/CMs tri-culture in the ratio of 4:1:5 with total cell concentration of 50M cells/ml.
3. GFP-tagged HUVECs/DPSCs/CMs/ RFP-tagged MΦs quad-culture in the ratio of 4:1:5:2 with total cell concentration of 60 M cells/ml.

The above cell combinations were mixed with human fibrinogen hydrogel (33mg/mL, Sigma-Aldrich).

Thrombin (0.5uL at 25U/mL) was added to the empty microwell before the seeding of the cell/gel mixture (2uL). Seeded tissues were cultured in I3M media (StemPro-34 complete media supplemented with 20mM HEPES, 1% GlutaMAX, and 213ug/mL 2-phosphate ascorbic acid) and EGM2 media (50:50) for 14 days with two media changes (100% of the volume) every week.

Sequential seeding: Initial seeding (inner core): GFP-tagged HUVECs/DPSCs at 4:1 with total cell concentration of 25M cells/ml.

The second seeding (outer layer) was seeded two days later with CMs only or CM/ RFP-tagged MΦs at 50M or 70 M cells/mL

Thrombin (0.5uL at 25U/mL) was added to the empty microwell before the seeding of the cell/gel mixture (2uL). Seeded tissues were cultured in I3M media (StemPro-34 complete media supplemented with 20mM HEPES, 1% GlutaMAX, and 213ug/mL 2-phosphate ascorbic acid) for 14 days with two media changes (100% of the volume) every week.

For sequential seeding co-culture, the first seeding containing EC/DPSC was done the same as single seeding tissues described above. The second seeding with CMs or CMs/ RFP-tagged MΦs was done two days after the initial seeding to allow the initial compaction of the tissue core. Prior to the second seeding, media in the well as well as the microwell was removed as much as possible by aspiration. Thrombin (0.5uL at 25 U/mL) was added to each microwell. After the CM and MΦs were thoroughly mixed and encapsulated within fibrinogen, 1uL of cell/gel mixture was spread within the microwell and formed layers

surrounding the initial seeded tissues. Cells were maintained in the mixture of I3M and EGM2 media (50:50) for 14 days.

Force characterization—Force characterization in the Biowire II platform was performed as previously reported[31]. Briefly, tissues were moved into a sterile electrical stimulation chamber connected with a Grass x88 stimulator for functional evaluation one week after seeding, as well as the endpoint. The excitation threshold (ET at 1Hz) and maximum capture rate (at 2xET) were assessed and recorded accordingly. The maximum displacements of the POMaC wires, that serve as anchor points of the tissue as well as force sensor via contraction induced displacement, were then recorded, and analyzed through the previously developed MATLAB code at 1Hz electrical pacing[31]. The forces of contraction and contractile dynamics were derived according to the force-displacement calibration curves through the MATLAB code, where active force, passive tension, duration of contraction, time to peak, time from peak, contraction slope, and relaxation slope were identified and summarized as described[31].

Cultivation of tissues in 384-well iFlow plate (Method S3)—IFlow plate (OrganoBiotech©) seeding was performed according to the manufacturer's instructions. For the first step of seeding, a mixture of HUVECs/DPSCs with a ratio of 5:1 and 5.76M cells/ml was mixed with 20µl human fibrinogen hydrogel (10mg/mL, Sigma-Aldrich) within a 1.5ml tube, for the cardiac organoids experiment, for cardiac organoids addition, 12 cardiac organoids with and without MΦs (760K cells/ml) were added to the cell mixture. followed by the addition of 5µl human thrombin (1U/ml, Sigma-Aldrich) to receive 25µl fibrin that was immediately casted into the middle well. followed by a 30-minute incubation at room temperature. Coating media containing EGM2 supplemented with 1mg/ml fibrinogen, 0.1U/ml thrombin and 20µg/ml aprotinin was then added to the wells (100µl to the two side wells and 40µl to the main well). The plate was then incubated flat in the incubator. 24 hours later, the media was replaced with EGM2 supplemented with 20µg/ml aprotinin. With 80µl of media in the main well and 50µl in each of the side wells. The plate was then incubated on a rocker with 15° tilting every 10 minutes. For the second seeding, 48 hours later, HUVECs (1M/ml) were seeded in the inlet and outlet wells with 110µl in the inlet and outlet well and 40µl in the main well. The plate was then incubated flat for 24 hours. iPSC-CMs (10M cells/ml) with and without MΦs (760K cells/ml) were then mixed in 50µl i3M/EGM2 media supplemented with 20µg/ml aprotinin and seeded into the main well. The plate was incubated flat for two hours followed by rocker incubation with 15° tilting every 10 minutes. Media containing 50% i3M and 50% EGM2 supplemented with 20µg/ml aprotinin was changed daily (50µl for the main well and 90µl for the inlet and outlet wells) and cultures were kept up to day 16. Followed by permeability test and fluospheres™ polystyrene microspheres, 10 µm, blue fluorescent (365/415) (Thermo Scientific, 20µl in 1ml of media) flow demonstration. Tissues were then fixed with 4% PFA over-night at 4C on a rocker with 15° tilting every 10 minutes, tissues were then washed three times with PBS, for 10 min for each wash, followed by PBS incubation overnight, followed by blocking 10%.

iFlow plate permeability test—Permeability of the vessels formed in the middle well of the iFlow plate was measured by perfusing TRITC-labelled dextran (1mg/ml media, 70 kPa, Sigma-Aldrich) through the vascular network, and quantifying the amount of dextran molecules passing through the vessels. Briefly, 90μl TRITC-labelled dextran was added to the inlet well dextran, 50μl of media was added to the main well, and the outlet well was left empty. At time = 0 min, 15 min, 60 min, and 120 min, fluorescence intensity of four regions of each middle well were measured by a SpectraMax i3 spectrophotometer (Molecular Devices). Diffusive permeability of the vessels, Pd, was calculated using the following equation reported by Rajasekar et al.[64], where Ii and If refers to the average intensities at final and initial timepoint, Ib refers to the average background intensities, Δt refers to the time interval, and d refers to the average diameter of the vessels.

$$P_d = \frac{1}{I_i - I_b}\left(\frac{I_f - I_i}{\Delta t}\right) \times \frac{d}{4}$$

Vascular morphology evaluation—The tissues in fibrin gels, biowire and iFlow platform were observed under the fluorescence microscope (Olympus IX81) every week and images were taken to evaluate the vascular formation within the tissues. The location and morphology of HUVECS (GFP-Green) and Mac (RFP-Red) were monitored to understand the dynamic nature of the formed tissues over time.

IF staining and confocal imaging—At the endpoint, tissues were fixed overnight at 4C in 4% PFA, permeabilized, and blocked using a blocking solution (0.1% triton X, 10% FBS in PBS) for 1hr before adding the primary antibodies. All staining incubation was performed at 4C. Mouse anti-α-actinin (1:200, Abcam Cat# ab137346, RRID:AB_2909405), rabbit-anti-MLC2v (1:200, Abcam Cat# ab79935, RRID:AB_1952220), Mouse-anti-Troponin-T (1:200, Thermo Fisher Scientific Cat# MA5-12960, RRID: AB_11000742) and mouse-anti-CD68 (1:200, Thermo Fisher Scientific Cat# 14-0688-82, RRID:AB_11151139) were applied for 48 hrs, followed by 24 hr washing in PBS solution, followed by 48 hrs of secondary antibody incubation. Goat-anti-rabbit Alexa Flour 647 (1:400, Thermo Fisher Scientific Cat# A32795, RRID:AB_2762835), and Goat anti-Rabbit Alexa Flour 555 (1:400, Thermo Scientific Cat# A32732, RRID:AB_2633281) and Goat anti-mouse Alexa Flour 647 (1:400, Thermo Fisher Scientific, Cat# A-21240, RRID:AB_2535809) were used as secondary antibodies. All tissues were counterstained with DAPI (1:1000, Thermo Fisher Scientific Cat# D1306, RRID:AB_2629482) for the nucleus. The tissues were imaged with a Leica light-sheet confocal microscope at 10x and 20x magnifications, and with Nikon A1R with 10x and 20x and 63X magnifications.

Histological analysis

H&E: In this study, histological analysis was conducted using the standard Hematoxylin and Eosin (H&E) staining procedure using Pathology Research Program at the Toronto General Hospital. Initially, slides were dewaxed and rehydrated through graded alcohols to water. Following rehydration, slides were washed under running tap water to prepare for staining. The staining process commenced with Harris Hematoxylin (Leica, 3801560) application for a period of 5 to 8 minutes, succeeded by a wash in tap water. Discrimination

of hematoxylin staining was achieved with a brief 1–2 dips in 0.5% acid alcohol, followed by a thorough rinse in tap water for 2 minutes. Slides were then treated with ammonia water for another 2 minutes and subsequently washed thoroughly in water for 5 minutes. Cytoplasmic components were then stained for 20 seconds using a 0.5% aqueous eosin solution (Fisher Scientific, Cat# E-511)., followed by a brief rinse in tap water. Post staining, slides underwent a dehydration process through graded alcohols and were cleared in xylene. Afterward, the slides were mounted with coverslips and labeled accordingly.

Immunohistochemical analysis

For double staining: Immunohistochemical analysis was performed for the detection of CD31 and CD68 antigens within 4μm thick formalin-fixed paraffin-embedded sections mounted on charged slides. The sections underwent dewaxing in xylene through five changes and were hydrated using a series of decreasing alcohol concentrations until water was reached. Endogenous peroxidase activity was blocked with 3% hydrogen peroxide.

Heat-Induced Epitope Retrieval (H.I.E.R) was employed using: Citrate pH 6.0, Tris-EDTA pH 9.0, Pepsin, and Trypsin solutions. Subsequently, a serum block from the MACH 2 Double-stain Cocktail kit was applied. The MACH 2 Doublestain Cocktail (Intermedico Cat# BC-MRCT525G) was then employed as instructed by the manufacturer to prevent non-specific binding. This was followed by the application of cocktail of primary antibodies; for CD68, a clone PG M1 from Dako (Agilent Cat# M0876, RRID:AB_2074844) was used with a low-temperature Tris-EDTA pH9.0 pretreatment and diluted to 1/300 for a 2-hour room temperature incubation resulting in a DAB reaction. CD31 was detected using a Novus antibody (Novus Cat# NB100-2284, RRID:AB_10002513) with no clone specified, diluted to 1/100, and also incubated at room temperature for 2 hours resulting in Warp Red visualization. The slides were then counterstained lightly with Mayer's Hematoxylin, dehydrated in graded alcohols, and cleared in xylene before being mounted with MM 24 Leica mounting medium (Cat#3801120).

For single staining: Endogenous peroxidase was blocked using a 3% hydrogen peroxide solution to prevent non-specific staining. Antigen retrieval was then performed using 10X stock of Citrate buffer pH 6.0 composed of Sodium Citrate and Citric Acid, a Tris-EDTA buffer pH 9.0 10X stock solution containing Tris and Ethylenediaminetetraacetic acid Disodium salt dehydrate, 1% Pepsin solution in 0.01 N HCl, and a 0.1% Trypsin solution in PBS, using heat-induced epitope retrieval (H.I.E.R) at temperatures ranging from 98–120°C or enzymatic retrieval methods. After antigen retrieval, the sections were treated with a serum block according to the ImmPress species-specific HRP kit protocol. Primary antibody was then applied, CD31 (Novus Cat# NB100-2284, RRID:AB_10002513) pretreated with citrate buffer, and diluted to 1/200 for overnight incubation. Followed by the application of ImmPress anti-Rabbit IgG kit (Cat# MP 7401) reagents as per the kit's instructions. Color development was achieved using DAB (DAKO Cat# K3468), which produces a brown coloration for the reaction products. Sections were counterstained with Mayer's Hematoxylin to label non-reactive nuclei in blue. Following counterstaining, the sections were dehydrated in graded alcohols, cleared in xylene, and finally mounted with MM 24 Leica mounting medium (Cat#3801120).

Image processing analysis: In order to examine the development of vessels, vessel's eccentricity and density were evaluated using a custom Matlab program[65]. Eccentricity serves as an indicator of how elliptical an object is, with perfectly round objects receiving a score of 0. As the shape becomes more compressed and elongated, the scores increase towards 1. Briefly, the images were converted into binary format, and the imageprops function was utilized to measure eccentricity. Eccentricity values were then divided into bins, and the percentage of elements that reached eccentricity values of 0.95–1 was plotted.

Using AngioTool software (the National Cancer Institute), average length of vessels, total number of vessel junctions and lacunarity (a measurement of how fractal features fill in the space) within the constructs were measured. A greater length of vessels and a higher count of vessel junctions with low lacunarity measurement were interpreted as signs of a more advanced and intricate network (Figure S1a).

LDH assay: Lactate dehydrogenase (LDH) release was measured for the two groups cultivated in fibrin hydrogel: EC/DPSC/CM/ MΦs and EC/DPSC/CM from the culture media samples collected at day 10 of culture, where the last media change was two days before. LDH quantity was quantified using LDH cytotoxicity assay kit (Cayman), according to the manufacturer's instructions.

Circulating cell-free mitochondrial DNA Measurement: Mitochondrial DNA was extracted from conditioned media of the two groups cultivated in fibrin hydrogel: EC/DPSC/CM/ MΦs and EC/DPSC/CM. Conditioned media samples (100μl) were collected at day 10 of culture, where the last media change was two days before. The QiaAMP DNA mini kit (Qiagen) was used according to the manufacturer's instructions. Followed by DNA elution with 100μL ultra-pure distilled water free from DNAse and RNAse (Invitrogen).

A commercially synthesized PCR product oligonucleotide (Integrated DNA Technologies), with a known concentration, was subjected to serial dilution to create a concentration range spanning from 108 to 102 copies/μL. This was employed to estimate the absolute concentration of cell-free circulating mtDNA (ccf-mtDNA). The mitochondrial genes ND4 and ND1 were selected to represent the major and minor arc of the mitochondrial genome, respectively.

A TaqManTM Duplex PCR assay was conducted on BioRad's C1000 Thermal cycle CFX96 Real Time System, employing a 20μL reaction mixture containing 10μL of TaqManTM Fast Advanced Master Mix (ThermoFisher), 4μL of DNA, 1μL of each Forward and Reverse primer, and 1μL of TaqManTM probe for each gene. The qPCR cycling conditions, as instructed by the manufacturer, consisted of an initial incubation at 50 o C for 2 minutes, followed by denaturation at 95 oC for 20s, 40 cycles of denaturation at 95 o C for 3 seconds, annealing at 60 oC for 30 seconds, and a fluorescent read per cycle.

Bulk RNA sequencing: RNA extraction from the 4 groups, cultivated in fibrin hydrogel: EC, EC/DPSC, and EC/DPSC/CM, and EC/DPSC/CM/MΦs at day 10 of culture, was done by using the PicoPure™ RNA Isolation Kit (Thermo Fisher Scientific KIT0204).

RNA sequencing was performed by Novogene as described below. After quality control analysis, messenger RNA was purified from total RNA using poly-T oligo-attached magnetic beads. After fragmentation, the first strand cDNA was synthesized using random hexamer primers, followed by the second strand cDNA synthesis using dTTP for non-directional library. The library was checked with Qubit and real-time PCR for quantification and bioanalyzer for size distribution detection. Quantified libraries were pooled and sequenced on an Illumina NovaSeq S4 with a read length of 2×150 paired-end reads to a depth of 20 million reads in each direction.

Fastq files were processed through fastp software for adapter and quality trimming as well as QC analyses. Trimmed reads were aligned to the reference human genome using Hisat2 v2.0.5. featureCounts v1.5.0-p3 was used to count the reads mapped to each gene and calculate FPKM. Differential expression analysis was performed using the DESeq2 R package (1.20.0) with a false discovery rate adjusted p-value <0.05 considered significant.

Additional analysis was performed using the following software: 1. Novomagic online analyzer (Novogene)- for differentially expressed gene list, PCA analysis, and gene clustering. 2. Morpheus, https://software.broadinstitute.org/morpheus, was used for plotting the heatmaps. 3.Enricher (Ma'ayan lab), an enrichment analysis tool was used to detect enriched pathways, 4. Go chord graph was plotted by https://www.bioinformatics.com.cn/en, a free online platform for data analysis and visualization. 5. All other graphs were plotted using prism.

Bulk RNA sequencing data have been archived at the short read archive at NCBI. The accession number is NCBI: GSE240488. (https://www.ncbi.nlm.nih.gov/geo/query/acc.cgi?acc=GSE240488).

snRNA sequencing: For snRNA sequencing, 3 groups of samples were used. 1) MΦs in suspension (1M cell pellet). 2) Day 10 fibrin tissues of EC/DPSC/CM (prepared as mentioned earlier in the text), where 10 samples were pooled together. 3) Day 10 fibrin tissues of EC/DPSC/CM/MΦ (prepared as mentioned earlier in the text), where 10 samples were pooled together.

10x sample preparation of macrophages suspension: 1 mL of cold lysis buffer comprising 0.32M Sucrose, 5mM CaCl2, 3mM Mg(Ac)2, 20mM Tris-HCl pH 7.5, 0.10% Triton X-100, 0.1mM EDTA pH 8.0, DEPC Water, 40U/mL RNase Inhibitor (Millipore Sigma, cat. No. 3335402001) was added to the frozen cell pellet for 5-minute lysis. The pellet was dissociated by pipette mixing. After the 5-minute lysis, nuclei were pelleted by spinning at 4C for 10 minutes at 800 × g. The supernatant was removed, and the nuclei pellet was resuspended with 2 mL wash buffer comprising 1x PBS, 1% BSA, and 0.1U/uL RNase Inhibitor. Centrifugation and resuspension with wash buffer was repeated for a total of 2 washes. After the second wash, the nuclei suspension was filtered using a 40um Flowmi cell strainer (Millipore Sigma, cat. no. BAH136800040). The purified nuclei suspension was centrifuged at 4C for 10 min at 800 rcf and the nuclei pellet was resuspended in wash buffer for a final nuclei concentration of 1000 nuclei/uL. Nuclei counting was done using AOPI (Revvity, cat. no. CS2-0106-25ML) on a haemocytometer (Thermo

Fisher, cat. no. 22-600-100). Following counting, the appropriate volume for each sample was calculated for a target capture of 10,000 cells and loaded onto 10x single cell G chip. After droplet generation, samples were transferred to a pre-chilled strip tube (USA Scientific, US14024700), and incubated in a Bio-Rad thermos cycler. Sample cDNA was recovered using Recovery Agent provided by 10x and subsequently cleaned up using a Silane DynaBead (Thermo Fisher) mix as outlined by the user guide 3' Reagent Kits v3.1. Purified cDNA was amplified for 11 cycles before being cleaned up using SPRIselect beads (Beckman Coulter). Samples were run on a Bioanalyzer (Agilent Technologies) to determine cDNA concentration. cDNA libraries were prepared as outlined by the Single Cell 3' Reagent Kits v3.1 user guide with modifications to the PCR cycles based on the calculated cDNA concentration.

Sequencing – The molarity of each library was calculated based on library size as measured bioanalyzer (Agilent Technologies) and qPCR amplification data (Roche, cat. no. 07960140001). Gene Expression libraries were sequenced on Illumina's NovaSeqX at the Princess Margaret Genomics Centre with the following run parameters: read 1 – 28 cycles, read 2 – 90 cycles, index 1 – 10 cycles and index 2 – 10 cycles.

10x sample preparation of tissue samples: Nuclei were isolated using 10x Genomics' Chromium Nuclei Isolation Kit (10x Genomics, cat. no. 1000493). The frozen tissue was transferred to a 2mL tissue grinder (Millipore Sigma, cat. no D8938). 500ul of Lysis buffer comprised of Lysis Reagent (10x Genomics, cat. no. 2000558), Reducing Agent B (10x Genomics, cat. no. 2000087), and Surfactant A (10x Genomics, cat. no. 2000559) was added to the frozen tissue on ice. The tissue was homogenized using 5 strokes with the loose pestle (pestle A) and 5 strokes with the tight pestle (pestle B). The sample was incubated on ice for a 10-minute lysis. At the end of the lysis incubation, the lysate was transferred to the Nuclei Isolation Column (10x Genomics, cat. no. 2000562) and spun at 16,000 rcf for 20 seconds at 4C. The supernatant was removed and the nuclei pellet was resuspended in Debris Removal Buffer comprised of Debris Removal Reagent (10x Genomics, cat. no. 2000560) and Reducing Agent B. The sample was spun at 700 rcf for 10 minutes at 4C. The supernatant was removed the purified nuclei pellet was washed twice with Wash Buffer comprised of 1x PBS, 10% BSA and RNase Inhibitor (Millipore Sigma, cat. No. 3335402001). The purified nuclei suspension was centrifuged at 4C for 5 min at 500 rcf and the nuclei pellet was resuspended in wash buffer for a final nuclei concentration of 1000 nuclei/uL. Nuclei counting was done using AOPI (Revvity, cat. no. CS2-0106-25ML) on a haemocytometer (Thermo Fisher, cat. no. 22-600-100). Following counting, the appropriate volume for each sample was calculated for a target capture of 10,000 cells and loaded onto 10x single cell G chip. After droplet generation, samples were transferred to a pre-chilled strip tube (USA Scientific, US14024700), and incubated in a Bio-Rad thermos cycler. Sample cDNA was recovered using Recovery Agent provided by 10x and subsequently cleaned up using a Silane DynaBead (Thermo Fisher) mix as outlined by the user guide 3' Reagent Kits v3.1. Purified cDNA was amplified for 11 cycles before being cleaned up using SPRIselect beads (Beckman Coulter). Samples were run on a Bioanalyzer (Agilent Technologies) to determine cDNA concentration. cDNA libraries were prepared as outlined

by the Single Cell 3' Reagent Kits v3.1 user guide with modifications to the PCR cycles based on the calculated cDNA concentration.

Sequencing – The molarity of each library was calculated based on library size as measured bioanalyzer (Agilent Technologies) and qPCR amplification data (Roche, cat. no. 07960140001). Gene Expression libraries were sequenced on Illumina's NovaSeqX with the following run parameters: read 1 – 28 cycles, read 2 – 90 cycles, index 1 – 10 cycles and index 2 – 10 cycles.

snRNA sequencing analysis: Samples were mapped individually then aggregated with cellranger (v7.2.0).

A human reference refdata-gex-GRCh38-2020-A downloaded from the 10x Genomics website was used.

Pre-processing and quality control: Analyses were performed in R v4.3.2. We first removed ambient RNA contamination using SoupX (v1.6.2)[66] with a contamination fraction set to 20% for the two groups: EC/DPSC/CM and EC/DPSC/CM/MΦ. Adjusted counts were used in downstream analyses using the Seurat package Seurat package (v5.0.1)[67–69]. Genes that were not detected in at least three cells were removed. Low quality cells with less than 200 expressed genes were excluded. Putative doublets or multiplets expressing a high number of genes (>8000) were removed. Cells expressing a high percentage of transcripts that map to mitochondrial genes (>20%) were considered potentially dead or lysed and were removed. The three datasets reported here were first pre-processed and filtered individually, and then subsequently merged for downstream analyses using the Seurat function 'merge'.

Normalization, dimensionality reduction, and clustering: We implemented the SCTransform function in Seurat for normalizing data, finding variable genes and scaling. Seurat utilizes regularized negative binomial regression and aims to remove technical variation while preserving biological variation. The variance- stabilizing transformation (vst) method was used to select the top 3000 highly variable features within the SCTransform function. We regressed out the number of counts (nCount_RNA) and the mitochondrial gene percentage. Principal component analysis (PCA) was used for linear dimensionality reduction, where the 20 most statistically significant PCs were used in downstream clustering. Data were integrated using Harmony[70] to correct for batch effects present across samples. We used the 'FindNeighbors' and 'FindClusters' functions to perform graph-based clustering, followed by non-linear dimensionality reduction and visualization using Uniform Manifold Approximation and Projection (UMAP). We performed differential gene expression analysis using the FindAllMarkers function to define and annotate cell types (Wilcoxon Rank Sum Test, min.pct: 0.25; logFC threshold: 0.25; adjusted p value < 0.05). Heatmaps were constructed using the top 30 differentially expressed genes (DEGs) where each cluster was downsampled to 50 cells for visualization.

Differential gene expression and pathway enrichment analysis across groups: To assess how each cell type changes in the presence or absence of macrophages, we used the 'subset' function to isolate each cell type. Then, we used the 'FindMarkers' function to compute

upregulated and downregulated DEGs across groups (Wilcoxon Rank Sum Test, min.pct: 0.25; logFC threshold: 0.25; adjusted P value < 0.05). Pathway enrichment analyses were performed using this gene set. Specifically, gProfiler (https://biit.cs.ut.ee/gprofiler/gost) was used to measure over-representation of our defined gene list against the Gene Ontology (GO) database (http://www.geneontology.org). We focused on enriched biological processes (BP), cell components (CC) and molecular processes (MP) of GO. We reported the -log10 of the adjusted P value as a measure of the enrichment score for each term.

NicheNet: receptor-ligand interaction analyses: We performed receptor-ligand interaction analysis using the R-based package NicheNet (v2.0.5)[42]. Macrophages were set as the 'sender' cell type. DPSCs, endothelial cells, fibroblasts and cardiomyocytes were each used as the 'receiver' cell types. The gene set of interest was defined as the DEGs upregulated in each receiver cell type in EC/DPSC/CM and EC/DPSC/CM/MΦ. Ligand activity analysis was performed, and the top predicted target genes and receptors were inferred from the top ligands. Receptors of top-ranked ligands were filtered bona fide ligand-receptor interactions documented in literature and publicly available databases.

To compare genes that appear in both snRNA sequencing and proteomics analysis, we used the InteractiVenn website[71], where the input was significantly different genes from both tests. Enriched pathways were detected using Enrichr[72].

Cytokine array: Media was collected from 3 pooled fibrin-based tissues from the two groups, EC/DPSC/CM/MΦ and EC/DPSC/CM, at day 10 of culture using the Raybiotech, Human L507 Array Glass Slide. Cytokines secretion measurement was performed according to the manufacturer's instructions. Slides were stored in a light-tight box prior to scanning using the Axon 4200A microarray scanner (Molecular Devices, Sunnyvale, CA). Photomultiplier tube (PMT) gain was manually adjusted to 370 and scanning power to 55% to sufficiently illuminate all positive control quadruplicate spots in the absence of fluorescence saturation using an 532nm excitation laser. Then, all slides were scanned at high resolution (10μm). Gene array list (GAL) visual analysis masks were automatically overlayed onto the scanned images then manually adjusted at each spot using the GenePix Pro software version 6.1.0.2 (Molecular Devices, Sunnyvale, CA). Fluorescence quantification at the masked spots and subsequent image optimization was automatically performed using GenePix Pro. The median fluorescence intensity observed following 532nm excitation was corrected for the local background signal at each spot yielding a corrected median fluorescence intensity (cMFI). Volcano plot and statistical tests were done using the Prism software, heatmap of the significant cytokines was generated using Morpheus, https://software.broadinstitute.org/morpheus.

Secretomics analysis: Phenol red-free conditioned media was collected from 3 pooled fibrin-based tissues from the two groups, EC/DPSC/CM/MΦ and EC/DPSC/CM, at day 10 of culture and was centrifuged at 2500*xg* for 20 minutes at 4°C to pellet any cell debris. The supernatant was collected and concentrated 10-fold using a 3 kDa molecular weight cut-off Amicon centrifuge filtration column (Millipore, Etobicoke, ON, Canada) at 4000*xg* for 1 hour at 4°C. Concentrates were dried down by vacuum centrifugation using a SpeedVac on medium heat for 2 hours (Thermo Fisher Scientific, Mississauga, ON, Canada). 20 μg

of conditioned media-derived proteins from each sample were denatured and reduced with 8 M urea, 10 mM DTT, 100 mM Tris-HCl pH 8.5 at 60°C for 30 minutes, followed by alkylation with 100 mM iodoacetamide for 15 minutes. The alkylation was attenuated by adding DTT to a final concentration of 40 mM and the urea in each sample was diluted to less than 1 M with 50 mM ammonium bicarbonate. The proteins were digested with 0.2 μg of trypsin (Sigma-Aldrich) overnight at 37°C. The resulting peptides were acidified and desalted using in-house C18 pipette tips. Analysis was performed on an Easy nLC-1200 coupled to a ThermoQExactive HF mass spectrometer (Thermo Fisher Scientific) operating in a Top 20 data-dependent acquisition mode. The mobile phase was composed of Buffer A (0.1% formic acid) and Buffer B (0.1% formic acid in 80% acetonitrile). Peptides were separated using a PepMap RSLC C18 2μm, 75μm × 50 cm column and a PepMap 100 C18 3μm, 75μm × 2cm precolumn with a 120-minute gradient of 5% to 40% Buffer B. Data were analyzed using MaxQuant (v1.6.10.43)[73] where specific tryptic peptides were detected at a false discovery rate (FDR) of 0.01 and label-free quantification (LFQ) was performed with default parameters. The identified and quantified protein groups were post-processed in Perseus (v1.6.5.0)[74] and the Cytoscape StringApp[75].

The mass spectrometry proteomics data have been deposited to the ProteomeXchange Consortium (http://proteomecentral.proteomexchange.org) via the PRIDE partner repository[62] with the dataset identifier PXD044560.

Quantification and Statistical Analysis—Statistical analysis was performed using with Prism 9.0 using one, two way ANOVA and repeated measures ANOVA or a t-test, as appropriate based on the data set and as indicated in the figure captions, with $p<0.05$ considered significant. With ANOVA Tukey or Bonferroni post-hoc tests were used. Normality and equality of variance was tested.

Supplementary Material

Refer to Web version on PubMed Central for supplementary material.

Acknowledgments

We would like to thank Prof. Stephen Juvet for the use of Axon 4200A microarray scanner and Michael Saikali for the advice on the proteomics. This work was funded by the National Institutes of Health Grant 2R01 HL076485, Natural Sciences and Engineering Research Council of Canada (NSERC) Discovery Grant (RGPIN 326982-10), NSERC Strategic Grant (STPGP 506689-17), Canadian Institutes of Health Research (CIHR) Foundation Grant (FDN-167274), Canada Foundation for Innovation/Ontario Research Fund grant 36442. M.R. was supported by Canada Research Chairs and Killam Fellowship. S.L. was supported by the Rothschild and EMBO (ALTF 530-2022) Fellowships. C.L.C was supported by Heart and Stroke Foundation of Canada grant G-22-0032216. S.A.S. was supported by a PRiME fellowship. S.E. was supported by CIHR, the Ted Rogers Centre for Heart Research and the Peter Munk Cardiac Centre.

References:

1. Montgomery M, Zhang B, and Radisic M (2014). Cardiac tissue vascularization: from angiogenesis to microfluidic blood vessels. Journal of cardiovascular pharmacology and therapeutics 19, 382–393. [PubMed: 24764132]
2. Banerjee I, Yekkala K, Borg TK, and Baudino TA (2006). Dynamic Interactions between Myocytes, Fibroblasts, and Extracellular Matrix. Ann N Y Acad Sci 1080, 76–84. [PubMed: 17132776]

3. Kuzuya M, and Kinsella JL (1994). Induction of endothelial cell differentiation in vitro by fibroblast-derived soluble factors. Exp Cell Res 215, 310–318. [PubMed: 7526993]
4. Dick SA, Macklin JA, Nejat S, Momen A, Clemente-Casares X, Althagafi MG, Chen J, Kantores C, Hosseinzadeh S, Aronoff L, et al. (2019). Self-renewing resident cardiac macrophages limit adverse remodeling following myocardial infarction. Nature immunology 20, 29–39. 10.1038/s41590-018-0272-2. [PubMed: 30538339]
5. Hulsmans M, Clauss S, Xiao L, Aguirre AD, King KR, Hanley A, Hucker WJ, Wulfers EM, Seemann G, Courties G, et al. (2017). Macrophages Facilitate Electrical Conduction in the Heart. Cell 169, 510–522 e520. 10.1016/j.cell.2017.03.050. [PubMed: 28431249]
6. Sugita J, Fujiu K, Nakayama Y, Matsubara T, Matsuda J, Oshima T, Liu Y, Maru Y, Hasumi E, Kojima T, et al. (2021). Cardiac macrophages prevent sudden death during heart stress. Nature Communications 12, 1910. 10.1038/s41467-021-22178-0.
7. Lavine KJ, Epelman S, Uchida K, Weber KJ, Nichols CG, Schilling JD, Ornitz DM, Randolph GJ, and Mann DL (2014). Distinct macrophage lineages contribute to disparate patterns of cardiac recovery and remodeling in the neonatal and adult heart. Proceedings of the National Academy of Sciences 111, 16029–16034.
8. Williams MAC, Mair DB, Lee W, Lee E, and Kim D-H (2022). Engineering three-dimensional vascularized cardiac tissues. Tissue Engineering Part B: Reviews 28, 336–350. [PubMed: 33559514]
9. Voges HK, Foster SR, Reynolds L, Parker BL, Devilée L, Quaife-Ryan GA, Fortuna PR, Mathieson E, Fitzsimmons R, and Lor M (2023). Vascular cells improve functionality of human cardiac organoids. Cell Reports.
10. Caspi O, Lesman A, Basevitch Y, Gepstein A, Arbel G, Habib IHM, Gepstein L, and Levenberg S (2007). Tissue engineering of vascularized cardiac muscle from human embryonic stem cells. Circulation research 100, 263–272. [PubMed: 17218605]
11. Sakaguchi K, Shimizu T, and Okano T (2015). Construction of three-dimensional vascularized cardiac tissue with cell sheet engineering. Journal of Controlled Release 205, 83–88. [PubMed: 25523520]
12. Noor N, Shapira A, Edri R, Gal I, Wertheim L, and Dvir T (2019). 3D printing of personalized thick and perfusable cardiac patches and hearts. Advanced science 6, 1900344. [PubMed: 31179230]
13. Mannhardt I, Marsano A, and Teuschl A (2021). Perfusion bioreactors for prevascularization strategies in cardiac tissue engineering. Vascularization for tissue engineering and regenerative medicine, 475–488.
14. Franklin RA (2021). Fibroblasts and macrophages: Collaborators in tissue homeostasis. Immunological reviews 302, 86–103. [PubMed: 34101202]
15. Zhou X, Franklin RA, Adler M, Jacox JB, Bailis W, Shyer JA, Flavell RA, Mayo A, Alon U, and Medzhitov R (2018). Circuit design features of a stable two-cell system. Cell 172, 744–757. e717. [PubMed: 29398113]
16. Atkins MH, Scarfò R, McGrath KE, Yang D, Palis J, Ditadi A, and Keller GM (2022). Modeling human yolk sac hematopoiesis with pluripotent stem cells. J Exp Med 219. 10.1084/jem.20211924.
17. Swirski FK, Robbins CS, and Nahrendorf M (2016). Development and function of arterial and cardiac macrophages. Trends in immunology 37, 32–40. [PubMed: 26748179]
18. Epelman S, Lavine KJ, Beaudin AE, Sojka DK, Carrero JA, Calderon B, Brija T, Gautier EL, Ivanov S, and Satpathy AT (2014). Embryonic and adult-derived resident cardiac macrophages are maintained through distinct mechanisms at steady state and during inflammation. Immunity 40, 91–104. [PubMed: 24439267]
19. Perry L, Ben-Shaul S, Landau S, and Levenberg S (2021). Co-culture systems for vasculogenesis. Vascularization for Tissue Engineering and Regenerative Medicine, 385–413.
20. Landau S, Guo S, and Levenberg S (2018). Localization of Engineered Vasculature within 3D Tissue Constructs. Front Bioeng Biotechnol 6, 2. 10.3389/fbioe.2018.00002. [PubMed: 29404324]

21. Guo S, Redenski I, Landau S, Szklanny A, Merdler U, and Levenberg S (2020). Prevascularized Scaffolds Bearing Human Dental Pulp Stem Cells for Treating Complete Spinal Cord Injury. Adv Healthc Mater 9, e2000974. 10.1002/adhm.202000974. [PubMed: 32902147]
22. Papetti M, Shujath J, Riley KN, and Herman IM (2003). FGF-2 antagonizes the TGF-β1-mediated induction of pericyte α-smooth muscle actin expression: a role for myf-5 and Smad-mediated signaling pathways. Investigative ophthalmology & visual science 44, 4994–5005. [PubMed: 14578427]
23. Li C, Issa R, Kumar P, Hampson IN, Lopez-Novoa JM, Bernabeu C, and Kumar S (2003). CD105 prevents apoptosis in hypoxic endothelial cells. Journal of cell science 116, 2677–2685. [PubMed: 12746487]
24. Welti J, Loges S, Dimmeler S, and Carmeliet P (2013). Recent molecular discoveries in angiogenesis and antiangiogenic therapies in cancer. The Journal of clinical investigation 123, 3190–3200. [PubMed: 23908119]
25. Distler J, Hirth A, Kurowska-Stolarska M, and Gay R (2003). Angiogenic and angiostatic factors in the molecular control of angiogenesis. The Quarterly Journal of Nuclear Medicine and Molecular Imaging 47, 149.
26. Litviňuková M, Talavera-López C, Maatz H, Reichart D, Worth CL, Lindberg EL, Kanda M, Polanski K, Heinig M, and Lee M (2020). Cells of the adult human heart. Nature 588, 466–472. [PubMed: 32971526]
27. Sim CB, Phipson B, Ziemann M, Rafehi H, Mills RJ, Watt KI, Abu-Bonsrah KD, Kalathur RK, Voges HK, and Dinh DT (2021). Sex-specific control of human heart maturation by the progesterone receptor. Circulation 143, 1614–1628. [PubMed: 33682422]
28. Zaman R, Hamidzada H, Kantores C, Wong A, Dick SA, Wang Y, Momen A, Aronoff L, Lin J, and Razani B (2021). Selective loss of resident macrophage-derived insulin-like growth factor-1 abolishes adaptive cardiac growth to stress. Immunity 54, 2057–2071. e2056. [PubMed: 34363749]
29. Dick SA, Wong A, Hamidzada H, Nejat S, Nechanitzky R, Vohra S, Mueller B, Zaman R, Kantores C, and Aronoff L (2022). Three tissue resident macrophage subsets coexist across organs with conserved origins and life cycles. Science immunology 7, eabf7777. [PubMed: 34995099]
30. Bajpai G, Schneider C, Wong N, Bredemeyer A, Hulsmans M, Nahrendorf M, Epelman S, Kreisel D, Liu Y, and Itoh A (2018). The human heart contains distinct macrophage subsets with divergent origins and functions. Nature medicine 24, 1234–1245.
31. Zhao Y, Rafatian N, Feric NT, Cox BJ, Aschar-Sobbi R, Wang EY, Aggarwal P, Zhang B, Conant G, and Ronaldson-Bouchard K (2019). A platform for generation of chamber-specific cardiac tissues and disease modeling. Cell 176, 913–927. e918. [PubMed: 30686581]
32. Offeddu GS, Haase K, Gillrie MR, Li R, Morozova O, Hickman D, Knutson CG, and Kamm RD (2019). An on-chip model of protein paracellular and transcellular permeability in the microcirculation. Biomaterials 212, 115–125. [PubMed: 31112823]
33. Dreher MR, Liu W, Michelich CR, Dewhirst MW, Yuan F, and Chilkoti A (2006). Tumor vascular permeability, accumulation, and penetration of macromolecular drug carriers. Journal of the National Cancer Institute 98, 335–344. [PubMed: 16507830]
34. Kemp M, Donovan J, Higham H, and Hooper J (2004). Biochemical markers of myocardial injury. British journal of anaesthesia 93, 63–73. [PubMed: 15096441]
35. Aristorena M, Gallardo-Vara E, Vicen M, de Las Casas-Engel M, Ojeda-Fernandez L, Nieto C, Blanco FJ, Valbuena-Diez AC, Botella LM, and Nachtigal P (2019). MMP-12, secreted by pro-inflammatory macrophages, targets endoglin in human macrophages and endothelial cells. International Journal of Molecular Sciences 20, 3107. [PubMed: 31242676]
36. Koenig AL, Shchukina I, Amrute J, Andhey PS, Zaitsev K, Lai L, Bajpai G, Bredemeyer A, Smith G, and Jones C (2022). Single-cell transcriptomics reveals cell-type-specific diversification in human heart failure. Nature cardiovascular research 1, 263–280.
37. Wald D, Qin J, Zhao Z, Qian Y, Naramura M, Tian L, Towne J, Sims JE, Stark GR, and Li X (2003). SIGIRR, a negative regulator of Toll-like receptor-interleukin 1 receptor signaling. Nat Immunol 4, 920–927. 10.1038/ni968. [PubMed: 12925853]

38. Hui X, Lam KS, Vanhoutte PM, and Xu A (2012). Adiponectin and cardiovascular health: an update. Br J Pharmacol 165, 574–590. 10.1111/j.1476-5381.2011.01395.x. [PubMed: 21457225]
39. Bourboulia D, Jensen-Taubman S, and Stetler-Stevenson WG (2012). TIMP-2: An endogenous angiogenesis inhibitor with distinct antitumoral properties. Treatment strategies. Hematology 2, 31.
40. Nunes SS, Miklas JW, Liu J, Aschar-Sobbi R, Xiao Y, Zhang B, Jiang J, Massé S, Gagliardi M, and Hsieh A (2013). Biowire: a platform for maturation of human pluripotent stem cell–derived cardiomyocytes. Nature methods 10, 781–787. [PubMed: 23793239]
41. Newman AC, Nakatsu MN, Chou W, Gershon PD, and Hughes CC (2011). The requirement for fibroblasts in angiogenesis: fibroblast-derived matrix proteins are essential for endothelial cell lumen formation. Molecular biology of the cell 22, 3791–3800. [PubMed: 21865599]
42. Browaeys R, Saelens W, and Saeys Y (2020). NicheNet: modeling intercellular communication by linking ligands to target genes. Nature methods 17, 159–162. [PubMed: 31819264]
43. Zhang B, Montgomery M, Chamberlain MD, Ogawa S, Korolj A, Pahnke A, Wells LA, Massé S, Kim J, and Reis L (2016). Biodegradable scaffold with built-in vasculature for organ-on-a-chip engineering and direct surgical anastomosis. Nature materials 15, 669–678. [PubMed: 26950595]
44. Lai BFL, Huyer LD, Lu RXZ, Drecun S, Radisic M, and Zhang B (2017). InVADE: integrated vasculature for assessing dynamic events. Advanced functional materials 27, 1703524.
45. King O, Cruz-Moreira D, Sayed A, Kermani F, Kit-Anan W, Sunyovszki I, Wang BX, Downing B, Fourre J, and Hachim D (2022). Functional microvascularization of human myocardium in vitro. Cell Reports Methods 2, 100280. [PubMed: 36160044]
46. Nicolás-Ávila JA, Lechuga-Vieco AV, Esteban-Martínez L, Sánchez-Díaz M, Díaz-García E, Santiago DJ, Rubio-Ponce A, Li JL, Balachander A, and Quintana JA (2020). A network of macrophages supports mitochondrial homeostasis in the heart. Cell 183, 94–109. e123. [PubMed: 32937105]
47. Hamidzada H, Pascual-Gil S, Wu Q, Kent GM, Massé S, Kantores C, Kuzmanov U, Gomez-Garcia MJ, Rafatian N, Gorman RA, et al. (2024). Primitive macrophages induce sarcomeric maturation and functional enhancement of developing human cardiac microtissues via efferocytic pathways. Nature Cardiovascular Research. 10.1038/s44161-024-00471-7.
48. Revelo XS, Parthiban P, Chen C, Barrow F, Fredrickson G, Wang H, Yücel D, Herman A, and van Berlo JH (2021). Cardiac resident macrophages prevent fibrosis and stimulate angiogenesis. Circulation research 129, 1086–1101. [PubMed: 34645281]
49. Zou L, Cao S, Kang N, Huebert RC, and Shah VH (2012). Fibronectin induces endothelial cell migration through β1 integrin and Src-dependent phosphorylation of fibroblast growth factor receptor-1 at tyrosines 653/654 and 766. Journal of Biological Chemistry 287, 7190–7202. [PubMed: 22247553]
50. Ingber DE (1990). Fibronectin controls capillary endothelial cell growth by modulating cell shape. Proceedings of the National Academy of Sciences 87, 3579–3583.
51. George EL, Georges-Labouesse EN, Patel-King RS, Rayburn H, and Hynes RO (1993). Defects in mesoderm, neural tube and vascular development in mouse embryos lacking fibronectin. Development 119, 1079–1091. [PubMed: 8306876]
52. Lyu Z, Jin H, Yan Z, Hu K, Jiang H, Peng H, and Zhuo H (2020). Effects of NRP1 on angiogenesis and vascular maturity in endothelial cells are dependent on the expression of SEMA4D. International Journal of Molecular Medicine 46, 1321–1334. [PubMed: 32945351]
53. Casazza A, Laoui D, Wenes M, Rizzolio S, Bassani N, Mambretti M, Deschoemaeker S, Van Ginderachter JA, Tamagnone L, and Mazzone M (2013). Impeding macrophage entry into hypoxic tumor areas by Sema3A/Nrp1 signaling blockade inhibits angiogenesis and restores antitumor immunity. Cancer cell 24, 695–709. [PubMed: 24332039]
54. Sakurai A, Doci C, and Gutkind JS (2012). Semaphorin signaling in angiogenesis, lymphangiogenesis and cancer. Cell research 22, 23–32. [PubMed: 22157652]
55. Guo S, Redenski I, Landau S, Szklanny A, Merdler U, and Levenberg S (2020). Prevascularized scaffolds bearing human dental pulp stem cells for treating complete spinal cord injury. Advanced healthcare materials 9, 2000974.

56. Medina-Leyte DJ, Domínguez-Pérez M, Mercado I, Villarreal-Molina MT, and Jacobo-Albavera L (2020). Use of human umbilical vein endothelial cells (HUVEC) as a model to study cardiovascular disease: A review. Applied Sciences 10, 938.
57. Mattei V, Martellucci S, Pulcini F, Santilli F, Sorice M, and Delle Monache S (2021). Regenerative potential of DPSCs and revascularization: direct, paracrine or autocrine effect? Stem cell reviews and reports, 1–12. [PubMed: 33423157]
58. Aurora AB, Porrello ER, Tan W, Mahmoud AI, Hill JA, Bassel-Duby R, Sadek HA, and Olson EN (2014). Macrophages are required for neonatal heart regeneration. J. Clin. Invest 124, 1382–1392. 72181 [pii];10.1172/JCI72181 [doi]. [PubMed: 24569380]
59. Lavine K, Epelman S, Uchida K, Weber K, Nichols C, Schilling J, Ornitz D, Randolph G, and Mann D (2014). Distinct Macrophage Lineages Contribute to Disparate Patterns of Cardiac Recovery and Remodeling in the Neonatal and Adult Heart. Proc. Natl. Acad. Sci 111, 16029–16034. [PubMed: 25349429]
60. Epelman S, Liu PP, and Mann DL (2015). Role of innate and adaptive immune mechanisms in cardiac injury and repair. Nature reviews. Immunology 15, 117–129. 10.1038/nri3800.
61. Lavine KJ, Epelman S, Uchida K, Weber KJ, Nichols CG, Schilling JD, Ornitz DM, Randolph GJ, and Mann DL (2014). Distinct macrophage lineages contribute to disparate patterns of cardiac recovery and remodeling in the neonatal and adult heart. Proceedings of the National Academy of Sciences of the United States of America 111, 16029–16034. 10.1073/pnas.1406508111. [PubMed: 25349429]
62. Perez-Riverol Y, Csordas A, Bai J, Bernal-Llinares M, Hewapathirana S, Kundu DJ, Inuganti A, Griss J, Mayer G, and Eisenacher M (2019). The PRIDE database and related tools and resources in 2019: improving support for quantification data. Nucleic acids research 47, D442–D450. [PubMed: 30395289]
63. Atkins MH, Scarfò R, McGrath KE, Yang D, Palis J, Ditadi A, and Keller GM (2021). Modeling human yolk sac hematopoiesis with pluripotent stem cells. Journal of Experimental Medicine 219, e20211924. [PubMed: 34928315]
64. Rajasekar S, Lin DS, Zhang F, Sotra A, Boshart A, Clotet-Freixas S, Liu A, Hirota JA, Ogawa S, and Konvalinka A (2021). AngioPlate–Biofabrication of perfusable complex tissues in multi-well plates with 4D subtractive manufacturing. bioRxiv, 2021.2008. 2013.456244.
65. Landau S, Shor E, Radisic M, and Levenberg S (2024). Quantitative Image Analysis of Tissue Properties: A MATLAB Tool for Measuring Morphology and Co-localization in 2D Images. bioRxiv, 2024.2004. 2003.587971.
66. Young MD, and Behjati S (2020). SoupX removes ambient RNA contamination from droplet-based single-cell RNA sequencing data. Gigascience 9, giaa151. [PubMed: 33367645]
67. Hao Y, Stuart T, Kowalski MH, Choudhary S, Hoffman P, Hartman A, Srivastava A, Molla G, Madad S, and Fernandez-Granda C (2023). Dictionary learning for integrative, multimodal and scalable single-cell analysis. Nature biotechnology, 1–12.
68. Hao Y, Hao S, Andersen-Nissen E, Mauck WM, Zheng S, Butler A, Lee MJ, Wilk AJ, Darby C, and Zager M (2021). Integrated analysis of multimodal single-cell data. Cell 184, 3573–3587. e3529. [PubMed: 34062119]
69. Stuart T, Butler A, Hoffman P, Hafemeister C, Papalexi E, Mauck WM, Hao Y, Stoeckius M, Smibert P, and Satija R (2019). Comprehensive integration of single-cell data. cell 177, 1888–1902. e1821. [PubMed: 31178118]
70. Korsunsky I, Millard N, Fan J, Slowikowski K, Zhang F, Wei K, Baglaenko Y, Brenner M, Loh P. r., and Raychaudhuri S (2019). Fast, sensitive and accurate integration of single-cell data with Harmony. Nature Methods 16, 1289–1296. 10.1038/s41592-019-0619-0. [PubMed: 31740819]
71. Heberle H, Meirelles GV, da Silva FR, Telles GP, and Minghim R (2015). InteractiVenn: a web-based tool for the analysis of sets through Venn diagrams. BMC bioinformatics 16, 1–7. [PubMed: 25591917]
72. Chen EY, Tan CM, Kou Y, Duan Q, Wang Z, Meirelles GV, Clark NR, and Ma'ayan A (2013). Enrichr: interactive and collaborative HTML5 gene list enrichment analysis tool. BMC bioinformatics 14, 1–14. [PubMed: 23323762]

73. Tyanova S, Temu T, and Cox J (2016). The MaxQuant computational platform for mass spectrometry-based shotgun proteomics. Nature protocols 11, 2301–2319. [PubMed: 27809316]

74. Tyanova S, Temu T, Sinitcyn P, Carlson A, Hein MY, Geiger T, Mann M, and Cox J (2016). The Perseus computational platform for comprehensive analysis of (prote) omics data. Nature methods 13, 731–740. [PubMed: 27348712]

75. Doncheva NT, Morris JH, Gorodkin J, and Jensen LJ (2018). Cytoscape StringApp: network analysis and visualization of proteomics data. Journal of proteome research 18, 623–632. [PubMed: 30450911]

Highlights

- Integrated four cell types to create vascularized cardiac tissue
- Assessed function using Biowire and iFlow organ-on-a-chip systems
- Primitive macrophages enhanced cardiac tissue functionality
- Primitive macrophages enhanced vessel stability, patency and perfusability

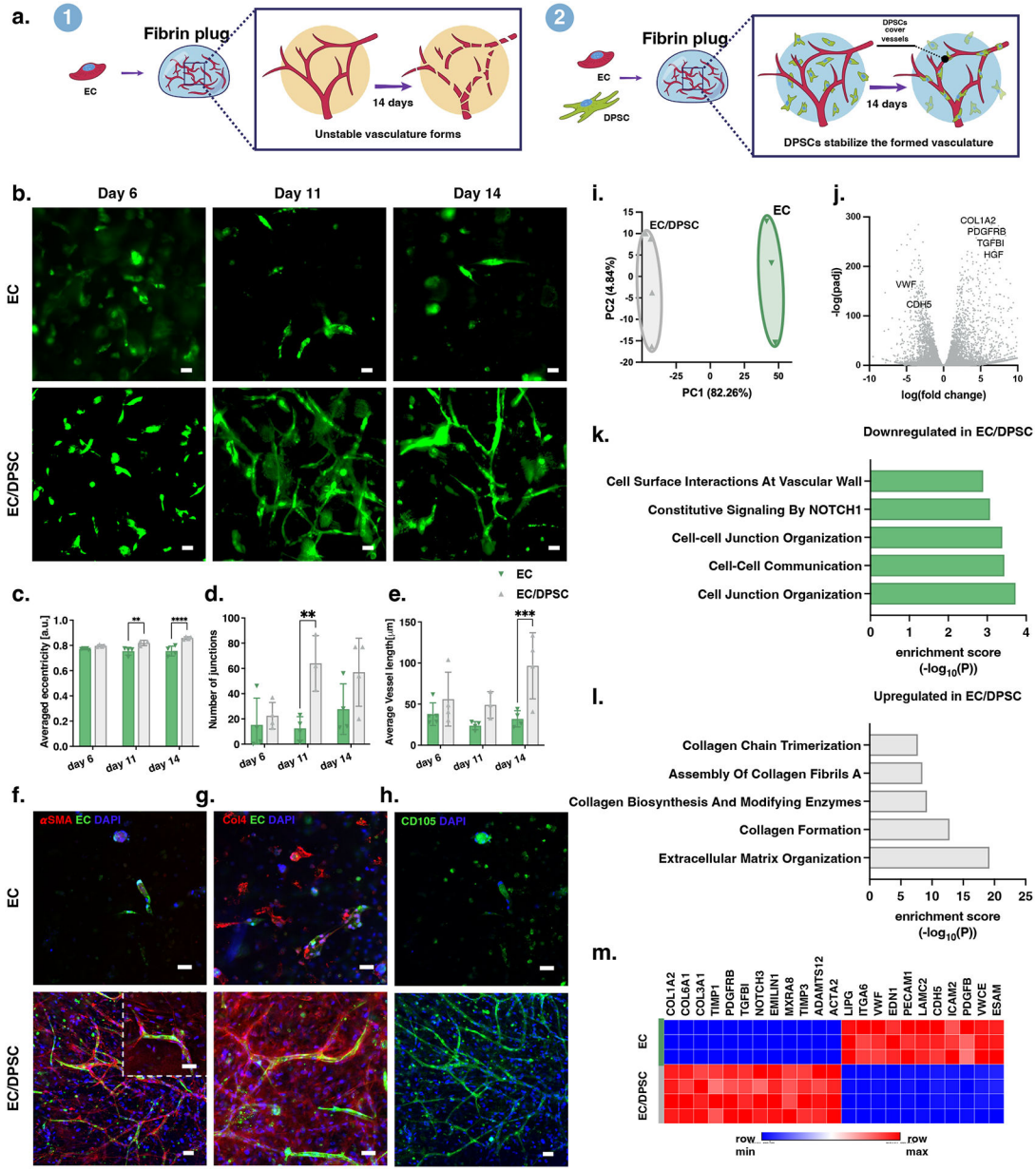

Figure 1: Establishment of microvasculature by co-culture of endothelial and stromal cells.

a) Schematics of the culture conditions of the tissues presented in this figure, ECs (1) or ECs and DPSCs (2) were cultured within a 3D fibrin hydrogel, incorporating DPSCs to the cell culture enables vessel stabilization over two weeks of culture. **b)** Representative images of day 6,11 and 14 live imaging of GFP+ EC monoculture and EC/DPSC co-culture within the fibrin hydrogel (GFP+ ECs shown in green). Scale bar=50 μm. **(c-e)** Quantification of vessel properties presented in b: **c)** vessel elongation, quantified by the eccentricity parameter, **d)** average vessel length, **e)** number of junctions. (All data is presented as mean ± SD, n ≥ 3 tissues per experiment, two-way ANOVA using Tukey's test, *P < 0.05, **P < 0.01, ***P < 0.001, ****P < 0.0001). **(f-h)** Representative images of immunostaining of day 14 EC vs. EC/DPSC fixed tissues of **f)** αSMA (red) and DAPI (blue). GFP+ ECs (green), **g)** Col4

(red) and DAPI (blue). Scale bar=50μm. and **h)** CD105 (green) and DAPI (blue), **i)** Principal component analysis (PCA) analysis of the genes analyzed in RNA sequencing from the two groups of tissues. **j)** Volcano plot of the upregulated and downregulated genes of the two groups. **k)** enriched pathways of the significant upregulated and **l)** downregulated genes. **m)** Heat map of the most upregulated and downregulated genes.

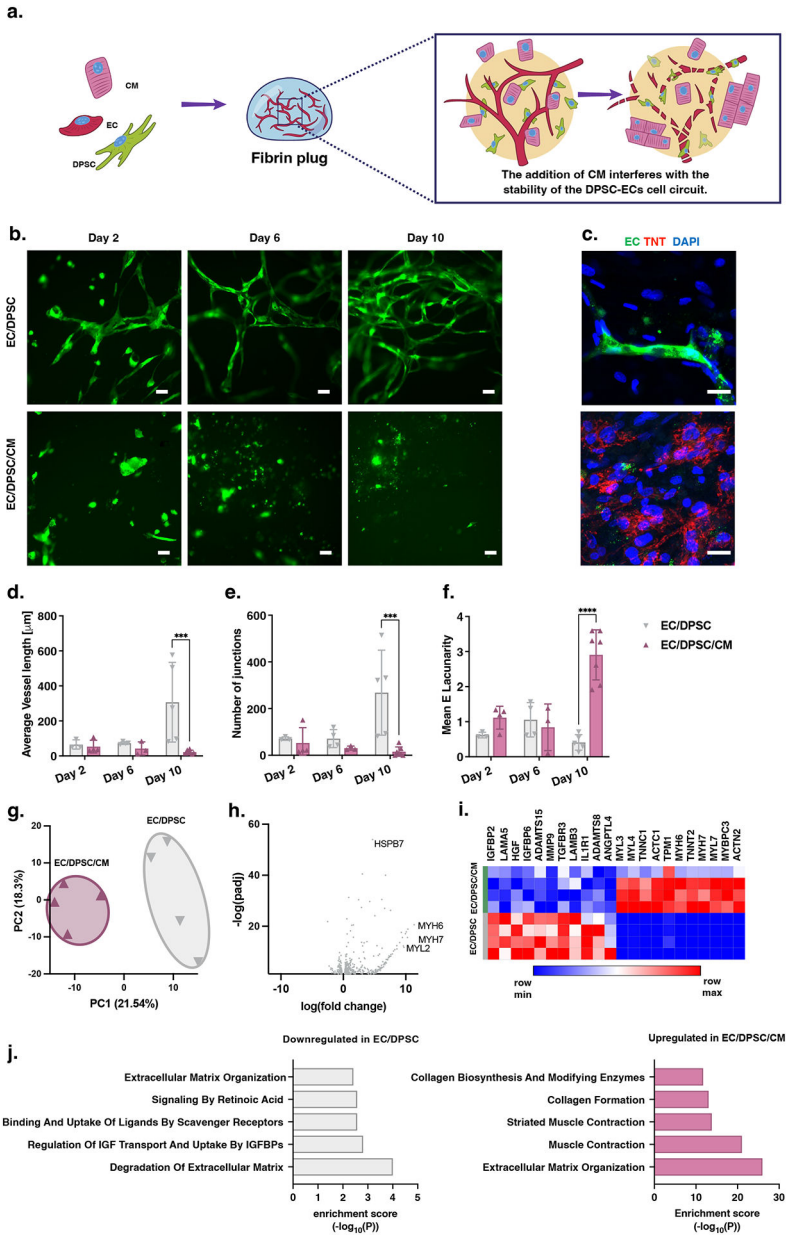

Figure 2: Incorporating CMs into the vascularized tissues results in cell-circuit homeostasis disruption.

a) Schematics of the culture conditions of the tissues presented in this figure, ECs and DPSCs were cultured within a 3D fibrin hydrogel, incorporating CMs (iPSC-BJ1D) to the tissues disrupts vessel formation. **b)** Representative imaging of day 2, 6, 8 and 10 live imaging of EC/DPSC in fibrin hydrogel with and without CMs. Scale bar=100 μm **c)** Representative images of immunostaining of day 10 EC/DPSC vs. EC/DPSC/CM fixed fibrin tissues of Cardiac troponin-T (red) and DAPI (blue). GFP+ ECs are presented in green. Scale bar=20 μm **(d-f)**. Quantification of vessel properties presented in b: **d)** average vessel length, **e)** number of junctions, **f)** mean E lacunarity. (All data is presented as mean ± SD, n ≥ 3 tissues per experiment, two-way ANOVA using Tukey's test, *P < 0.05, ***P < 0.001, ****P < 0.0001). **g)** PCA analysis of the RNA sequencing data from the two groups

of tissues. **h)** Volcano plot of the upregulated and downregulated genes of the two groups. **i**) heat map of the top upregulated and downregulated genes. **j)** enriched pathways of the significant upregulated and downregulated genes.

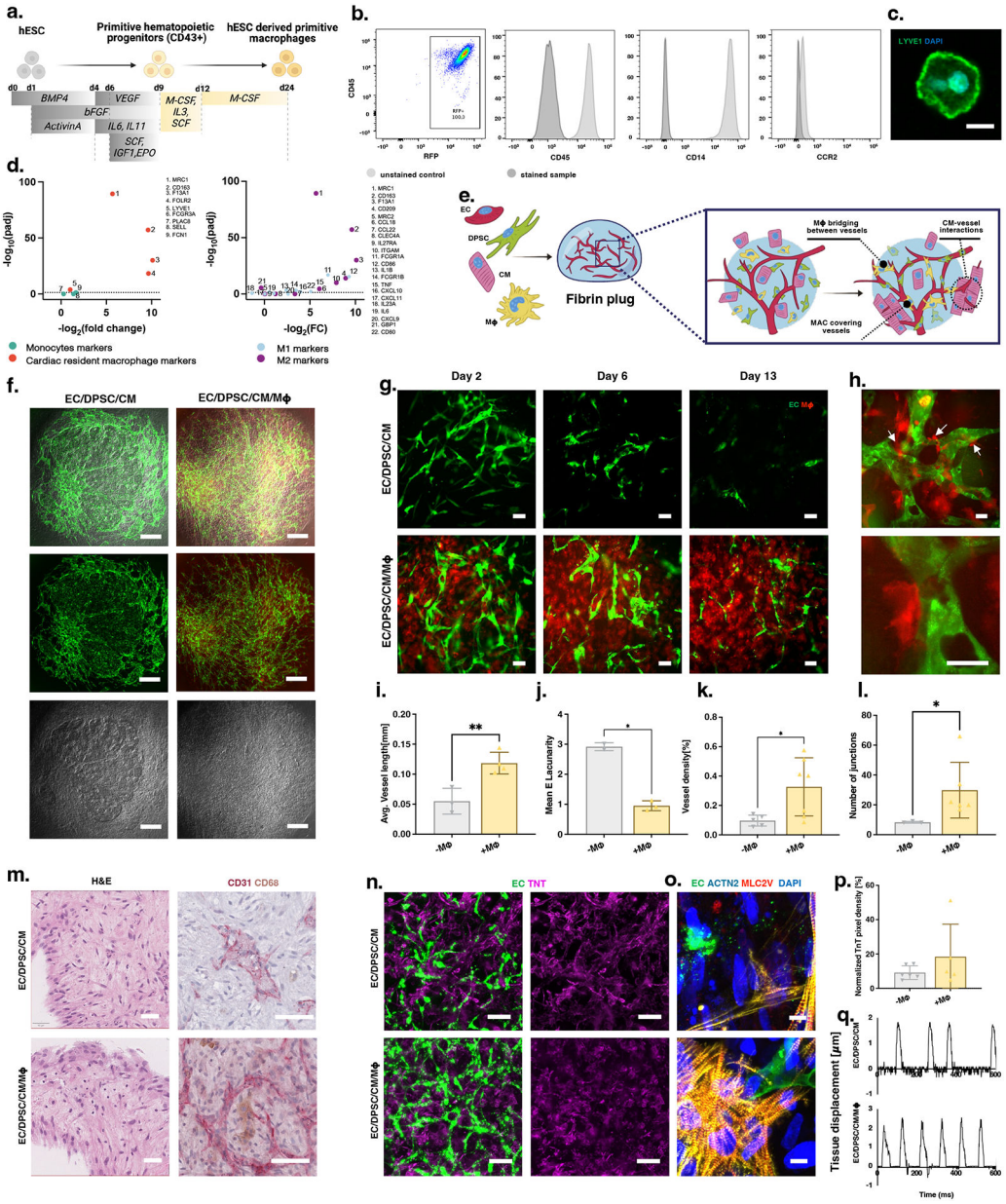

Figure 3: Restoring cell-circuit homeostasis within vascularized cardiac tissues is achieved through the incorporation of primitive macrophages.

a) Schematic of human embryonic stem cells (hESC)-primitive MΦ differentiation process**,** **b)** CD45, CD14, and CCR2 FACS analysis of the C-MΦs on day 24 of differentiation. **c**) LYVE-1 (green) immunostaining of hESC-MΦs on day 24 of differentiation. Scale bar=10 μm. **d)** Left: Adjusted p-value (Padj) versus fold change of monocyte markers and cardiac-resident macrophage markers. Right: adjusted p-value (Padj) versus fold change of M1 and M2 markers, from bulk RNA sequencing of tissues incorporated with MΦs versus tissues without them. **e)** Schematic of the cell culture seeding procedure of the tissues presented in this figure, EC/DPSC/iPSC-BJ1D-CM were cultured within a 3D fibrin hydrogel, incorporating MΦs to the tissues, resulting in vessel stabilization. **f)** Low magnification live cell imaging of a fibrin 3D hydrogel seeded with EC/DPSC/CM with and

without MΦs (GFP+ ECs are presented in green, RFP+ MΦs are presented in red, brightfield in gray), scale bar= 500 μm**. g)** Representative images of day 2, 6, 8, and 13 live-cell imaging of tissues in fibrin hydrogel with and without MΦs. (GFP+ ECs are presented in green and RFP+ MΦs are presented in red) Scale bar=100 μm. **h)** High magnification live cell imaging of a fibrin 3D hydrogel seeded with EC/DPSC/CM/ MΦs, white arrows demonstrate the various interactions of MΦs with the vessel network, such as bridging and wrapping. (GFP+ ECs are presented in green, and RFP+ MΦs are presented in red). Scale bar=25 μm **(i-l)** Quantification of vessel properties presented in **g**: **i)** average vessel length, **j)** mean E lacunarity, **k)** vessel density, and **l)** number of junctions. (All data are presented as mean ± SD, n ≥ 3 tissues per experiment, unpaired two-tailed t-test, *P < 0.05). **m)** Representative images of paraffin-embedded sections of H&E, CD31 (pink), CD68 (brown) staining of EC/DPSC/CM with and without MΦ tissues, fixed on day 10 of culture. Scale bar for H&E=50μm, Scale bar for CD31= 100μm **n)** Representative images of immunostaining of day 13 EC/DPSC/CM vs. EC/DPSC/CM/MΦ fixed fibrin tissues of TnT (magenta), (GFP+ ECs are presented in green) Scale bar=100 μm. **o)** Representative images of immunostaining of day 13 EC/DPSC/CM vs. EC/DPSC/CM/MΦ fixed fibrin tissues of TnT (yellow), MLC2V (red) and DAPI (blue), (GFP+ ECs are presented in green) Scale bar=10 μm. **p)** Quantification of TnT density staining; red pixels were counted and normalized to total image pixels. n≥5 tissues per group. **q)** Beating traces of the EC/DPSC/CM and EC/DPSC/CM/MΦs fibrin tissues.

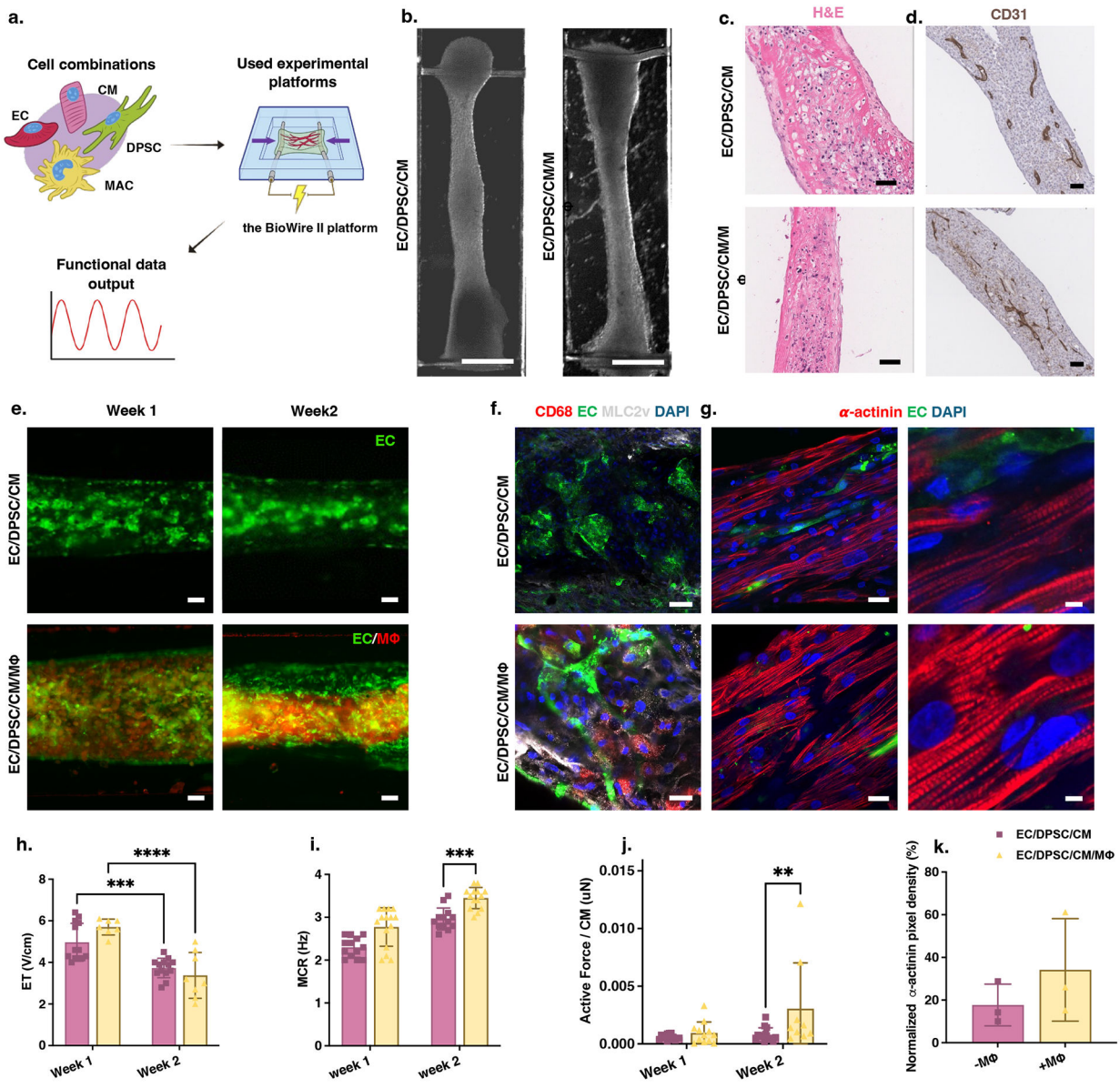

Figure 4: Primitive macrophages improve functional properties of vascularized cardiac tissues.

a) Schematic of the cell combination simultaneously seeded in the biowire. **b)** Representative bright filed images of Biowire tissues seeded with EC/DPSC/CM with and without MΦ on day 14 of culture. Scale bar=500 μm. **c)** Representative images of paraffin-embedded tissue sections using H&E staining of Biowire tissues seeded with EC/DPSC/CM with and without MΦ, where tissues were fixed on day 14 of culture. Scale bar=100 μm. **d)** Representative images of paraffin-embedded sections CD31 staining (brown) of Biowire tissues seeded with EC/DPSC/CM with and without MΦ, where tissues were fixed on day 14 of culture. Scale bar=50 μm. **e)** Representative images of EC/DPSC/CM biowire tissues with and without MΦ at weeks 1 and 2 of culture. (GFP+ ECs shown in green and RFP+ MΦs shown in red), scale bar=100 μm. **f)** Representative images of CD68 (red), MLC2V (gray), and DAPI (blue) immunostaining of EC/DPSC/CM with and without MΦs tissues

grown for 14 days, Scale bar=50 μm **g) Right:** Representative images of α-actinin (red) and DAPI (blue) immunostaining of EC/DPSC/CM with and without MΦs tissues grown for 14 days (GFP+ ECs shown in green) Scale bar=25μm, **left:** higher magnification of the image shown in panel d, Scale bar=5 μm. (**h-k)** Electrical and mechanical properties of EC/DPSC/CM with and without MΦs tissues measured on weeks 1 and 2 of culture, **h)** excitation threshold (ET), **i)** maximum capture rate (MCR), **j)** active force normalized to the input number of CMs, (All functional properties data are presented as mean ± SD, n >9 tissues, two-way ANOVA using Tukey's test, *P < 0.05, **P < 0.01). **k)** Quantification of α-actinin density staining; red pixels were counted and normalized to total image pixels. n=3 tissues per group. All CMs in this figure are derived from iPSC-BJ1D.

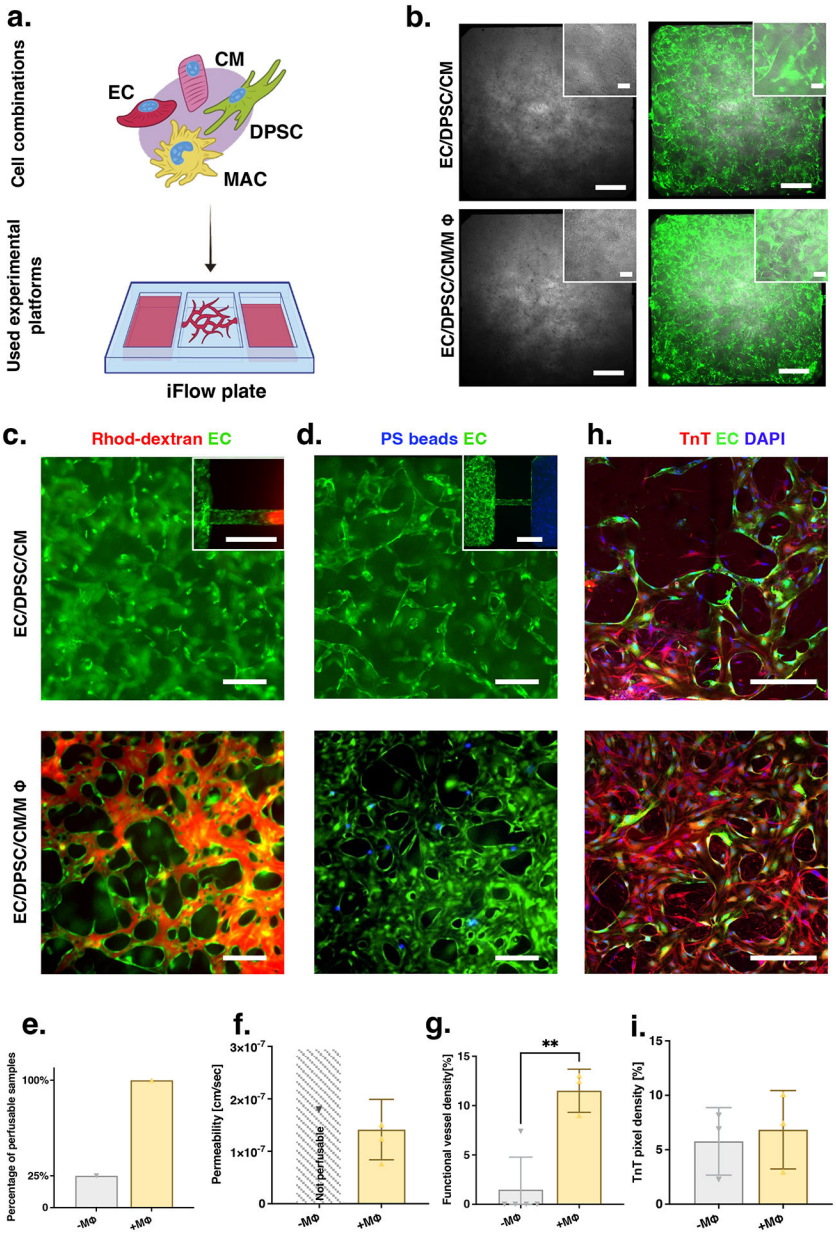

Figure 5: Primitive macrophages enable the formation of perfusable patent vessels in vascularized cardiac tissues.

a) Schematic of the cell combination seeded in the iFlow plate. **b)** Representative BF (left) and BF and fluorescent image (right) of an entire well in the iFlow plate seeded with EC/DPSC/CM tissues with and without MΦ and cultured for 14 days. Scale bar= 500 μm for the large images and 100 μm for the inset images. (**c-d)** Representative images of EC/DPSC/CM tissues with and without MΦ seeded in the iFlow plate demonstrating perfusability with **c)** rhodamine-dextran (red) perfused on day 11 of culture and **d)** 405-polystrene beads (blue) on day 16 of culture. (GFP+ ECs are shown in green). **e)** Percentage of perfusable tissues. n = 4 tissues. **f)** Permeability measurement of Rhodamine-dextran perfusion through the tissues on day 16 of culture. **g)** Quantification of the percentage of vessels that were perfused with rhodamine-dextran. (All data in this figure are presented as mean ± SD, n = 4

tissues per experiment, unpaired two-tailed t-test, *P < 0.05, **P < 0.01). **h)** Representative images of TnT (red) and DAPI (blue) immunostaining of iFlow plate tissues fixed on day 16 of culture. (GFP+ ECs are shown in green). Scale bar=250 μm**. i)** Quantification of TnT staining, red pixels were counted and normalized to total image pixels. n=3 tissues per group. All CMs in this figure are derived from iPSC-BJ1D.

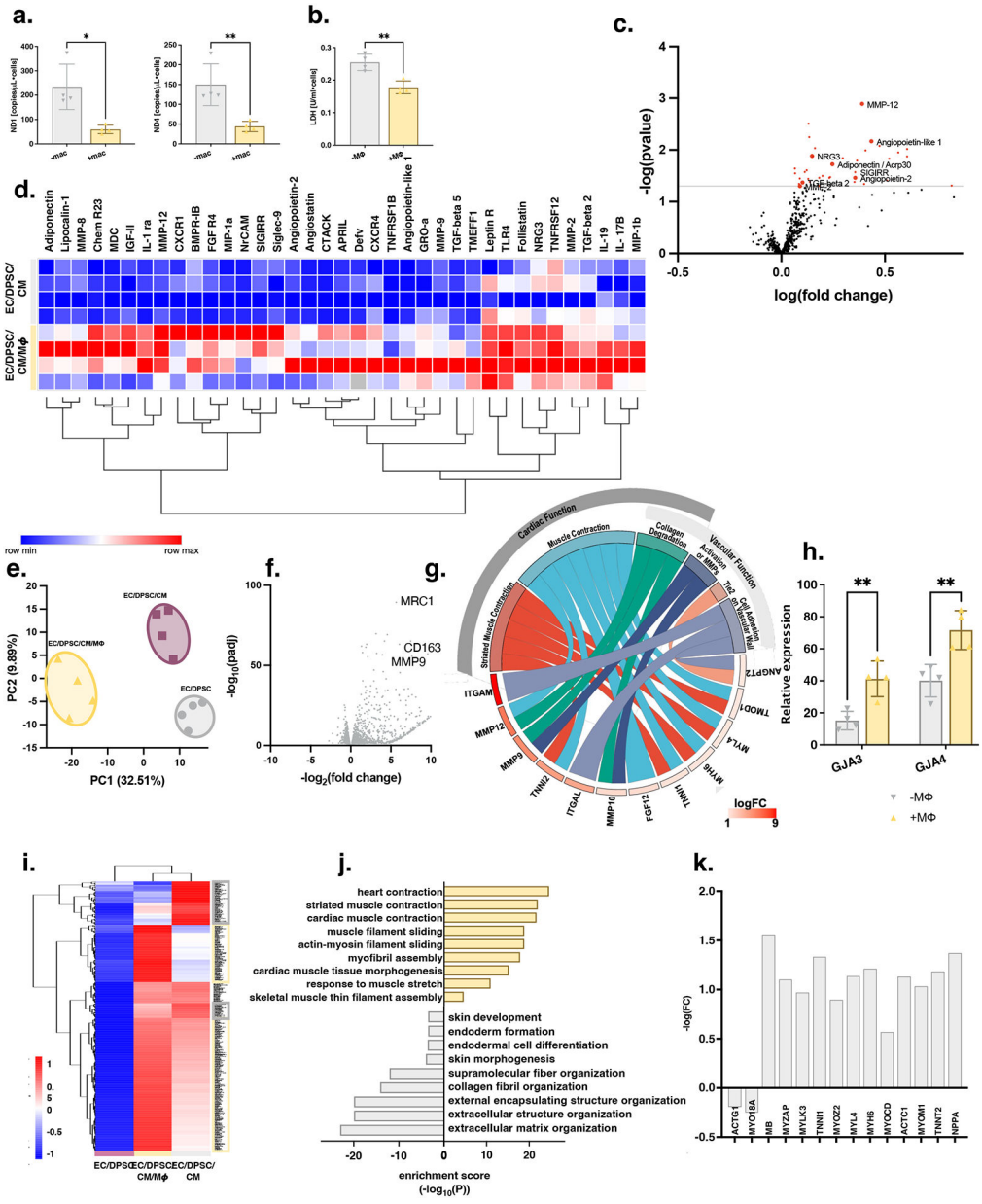

Figure 6: Primitive MΦs decrease cell damage markers, amplify pro-angiogenic cytokine secretome in vascularized cardiac tissues and enhance upregulation of pro-angiogenic and cardiac-associated genes demonstrated by bulk RNA sequencing.

a) ND1 and ND4 gene expressions were measured from day 14 conditioned media of EC/DPSC/CM and EC/DPSC/CM/MΦ fibrin tissues. Data are presented as mean ± SD, n = 4 tissues, unpaired two-tailed t-test, *P < 0.05, **P < 0.01. **b)** Measured secreted LDH from day 14 conditioned media of EC/DPSC/CM and EC/DPSC/CM/MΦ fibrin tissues. Data are presented as mean ± SD, n = 4 tissues, unpaired two-tailed t-test, **P < 0.01. **c)** Volcano plot of cytokines secreted from day 14 conditioned media of EC/DPSC/CM and EC/DPSC/CM/MΦ fibrin tissues. n = 4 tissues per group. **d)** heat map of significantly different cytokines between the two groups from plot **c**. **e-m)** RNA sequencing data was extracted from EC/DPSC, EC/DPSC/CM, and EC/DPSC/CM/MΦ fibrin tissues cultured

for 10 days *in vitro*. n=4 tissues per group. All CMs in this figure are derived from iPSC-BJ1D. **e)** Principal component analysis of the two vascularized cardiac tissue groups (with and without MΦ) and a control consisting of EC/DPSC alone. **f)** Volcano plot of the upregulated and downregulated genes, **g)** Enriched pathways with the matching genes involved in the processes that are significantly upregulated in the EC/DPSC/CM/MΦ group. **h)** Gap junction gene expression within the two groups. Data is presented as mean ± SD, n =4 tissues per group, unpaired two-tailed t-test, **Padj< 0.01, ***Padj < 0.001. **i)** Heat map clustering of the three groups according to the genes that are significantly upregulated in the EC/DPSC/CM versus EC/DPSC group. **j)** Enriched pathways based on the significantly differentially expressed genes in **i**, yellow indicates upregulated pathways based on the upregulated genes, and gray represents the enriched pathways based on the downregulated genes. **k**) Upregulated and downregulated of statistically significant differential expression of cardiac tissue-related genes. Padj<0.05

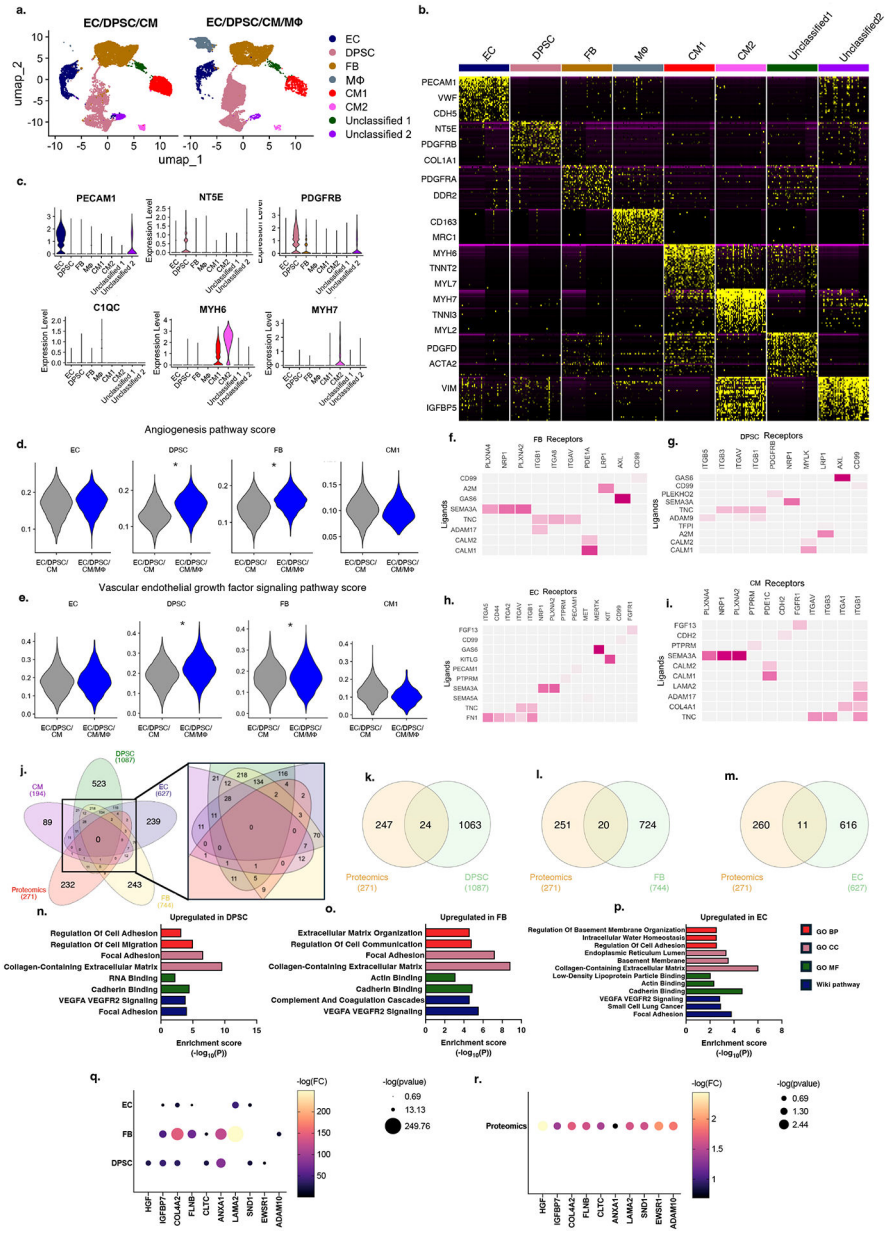

Figure 7: snRNA sequencing indicates that primitive macrophages enhance the stability of vascularized cardiac tissues via ECM and integrin interactions, corroborating proteomic analyses.

a) UMAP plots of the two tissue conditions, EC/DPSC/CM, with and without MΦs. **b)** Heatmap of the DEG of each cluster. **c)** Selected canonical genes plotted against each cluster**. d)** Angiogenesis pathway score within EC, DPSC, FB, and CM. **e)** VEGF signaling pathway score within EC, DPSC, FB, and CM. (**f-i)** NicheNet analysis of the receptor ligand interactions based on the DEG analysis of the two groups where ligands are coming from MΦs and receptors from **f)** FB, **g)** DPSC, **h)** EC, and **i)** CM. **(j-m)** Venn diagrams of DEG from snRNA sequencing data and proteomics data considering the overlap in **j)** Proteomics and all cells, **k)** Proteomics and DPSC, **l)** Proteomics and FB, and **m)**Proteomics and EC, **(n-p)** Top upregulated pathways from the DEG that are present both in proteomics and snRNA

sequencing data. **n)** Upregulated in DPSC, **o)** Upregulated in FB, and **p)** Upregulated in EC, **q)** Presentation of -log(Fold Change) using color gradients and -log(p-value) using dot sizes, indicating changes in selected genes from snRNA sequencing data. The data, presented in panels k-n, relate to angiogenesis, basement membrane, and VEGFR signaling, and identify the specific cells responsible for secreting each factor. **r)** Presentation of the -log(Fold Change) by the color gradient of dots and the -log(p-value) by the size of dots, showcasing changes in selected angiogenesis, basement membrane, and VEGFR signaling genes from the proteomics data in panels n-p.

Key Resources Table

REAGENT or RESOURCE
Antibodies
mouse anti-human CD14, clone M5E2
mouse anti-human CCR2, clone K036C2
Mouse anti-α-actinin
rabbit-anti-MLC2v
Mouse-anti-Troponin-T
mouse-anti-CD68
Goat-anti-rabbit Alexa Flour 647
Goat anti-Rabbit Alexa Flour Plus 555
Goat anti-mouse Alexa Flour 647
DAPI
Rabbit Anti CD31
Mouse Anti CD68
DAB
Warp Red
Mouse monoclonal anti-human CD45-BV605 (clone HI30)
Mouse monoclonal anti-human CD64-APCCy7 (clone 10.1)
Mouse monoclonal anti-human CD68-PECy7 (clone Y1/82A)
Chemicals, peptides, and recombinant proteins
pepsin
Polyurethane casting and potting system
carbon rods
Critical commercial assays
iFlowPlate
PicoPure RNA Isolation Kit
RNase-Free DNase Set
MACH 2 Doublestain Cocktail
Human L507 Array, Glass Slide

REAGENT or RESOURCE
LDH Cytotoxicity assay
CD34
Deposited data
mass spectrometry proteomics data
Bulk RNA sequencing data
snRNA sequencing data
Experimental models: Cell lines
iCell Cardiomyocytes
GFP Expressing Human Umbilical Vein Endothelial Cells
DPSC - Human Dental Pulp Stem Cells
Human ESC: HES2 line
tdRFP variant of the HES2
BJ1D cell line
Oligonucleotides
ND4- F1 5’-CCATTCTCCTCCTATCCCTCAAC-3’
ND4- R1 5’-ACAATCTGATGTTTTGGTTAAACTATATTT-3’
ND4- Probe 5’-FAM/CCGACATCA/ZEN/TTACCGGGTTTTCCTCTTG/3IABkFQ/-3’
ND1- F1 5’-CCCTAAAACCCGCCACATCT-3’
ND1- R1 5’-GAGCGATGGTGAGAGCTAAGGT-3’
ND1- Probe 5’-HEX/CCATCACCC/ZEN/TCTACATCACCGCCC/3IABkFQ/-3’
ND4 + ND1 geneblock - 5’-CACGAGAAAACACCCTCATGTTCATACACCTATCCCCCATTCTCCTCCTATCCCTCAACCCCGACATCATTACCGGGTTTTCCTCTTGTAAATATAGTTTAACCAAAAC
Software and algorithms
Image Analysis Matlab Code
Other
TrypLE
L-glutamine
transferrin
ascorbic acid
monothioglycerol
ROCK inhibitor Y-27632

REAGENT or RESOURCE
rhBMP4
rhActivinA
rhbFGF
rhVEGF
Recombinant MCSF
Recombinant IL3
Recombinant SCF
Recombinant human IL6
Recombinant human IL11
Recombinant human IGF-1
Aprotinin from bovine lung
StemPro™-34 SFM
EGM2
Aprotinin from bovine lung
StemPro™-34 SFM
RPMI with L-Glutamine
B27 plus insulin
B27 supplement minus insulin 50X
mTesr
2-Phospho-L-ascorbic acid trisodium salt
IWP4
CHIR 99021
NaOH
Na HCO_3
Growth factor reduced matrigel
Collagenase type 2
All trans RA
Retinol
DMEM
fetal bovine serum (FBS)
Penicillin-Streptomycin
Human fibrinogen
Human Thrombin
Trypsin/EDTA 0.05%

REAGENT or RESOURCE
Low glucose DMEM
FBS
MEM Non-Essential Amino Acids Solution (100X)
HEPES
GlutaMAX
Fluospheres™ Polystyrene Microspheres, 10 μm, blue fluorescent (365/415), for blood flow determination
Tetramethylrhodamine isothiocyanate-Dextran
triton X-100
MM 24 mounting medium
Fluospheres™ Polystyrene Microspheres, 10 μm, blue fluorescent (365/415), for blood flow determination